Available online at www.sciencedirect.com
ScienceDirect
Geochimica et Cosmochimica Acta 72 (2008) 2198–2216
Geochimica et Cosmochimica Acta
www.elsevier.com/locate/gca

Modeling fractional crystallization of group IVB iron meteorites

Richard J. Walker [a,*], William F. McDonough [a], Jenise Honesto [a], Nancy L. Chabot [b], Timothy J. McCoy [c], Richard D. Ash [a], Jeremy J. Bellucci [a]

[a] Department of Geology, University of Maryland, College Park, MD 20742, USA
[b] The Johns Hopkins University Applied Physics Laboratory, 11100 Johns Hopkins Road, Laurel, MD 20723, USA
[c] Department of Mineral Sciences, National Museum of Natural History, Smithsonian Institution, Washington, DC 20560-0119, USA

Received 28 March 2007; accepted in revised form 24 January 2008; available online 14 February 2008

Abstract

A ^{187}Re–^{187}Os isochron including data for all twelve IVB irons gives an age of 4579 ± 34 Ma with an initial $^{187}Os/^{188}Os$ of 0.09531 ± 0.00022, consistent with early solar system crystallization. This result, along with the chemical systematics of the highly siderophile elements (HSE) are indicative of closed-system behavior for all of the HSE in the IVB system since crystallization.

Abundances of HSE measured in different chunks of individual bulk samples, and in spot analyses of different portions of individual chunks, are homogeneous at the ±10% level or better. Modeling of HSE in the IVB system, therefore, is not impacted by sample heterogeneities. Concentrations of some other elements determined by spot analysis, such as P, Cr and Mn, however, vary by as much as two orders of magnitude and reflect the presence of trace phases.

Assuming initial S in the range of 0 to 2 wt.%, the abundances of the HSE Re, Os, Ir, Ru, Pt, Rh, Pd and Au in bulk IVB irons are successfully accounted for via a fractional crystallization model. For these elements, all IVB irons can be interpreted as being representative of equilibrium solids, liquids, or mixtures of equilibrium solids and liquids.

Our model includes changes in bulk *D* values (ratio of concentration in the solid to liquid) for each element in response to expected increases in S and P in the evolving liquid. For this system, the relative *D* values are as follow: Os > Re > Ir > Ru > Pt > Rh > Pd > Au. Osmium, Re, Ir and Ru were compatible elements (favor the solid) throughout the IVB crystallization sequence; Rh, Pd and Au were incompatible (favor the liquid). Extremely limited variation in Pt concentrations throughout the IVB crystallization sequence requires that *D*(Pt) remained at unity.

In general, *D* values derived from the slopes of logarithmic plots, compared with those calculated from recent parameterizations of *D* values for metal systems are similar, but not identical. Application of *D* values obtained by the parameterization method is problematic for comparisons of the compatible elements with similar partitioning characteristics. The slope-based approach works well for these elements. In contrast, the slope-based approach does not provide viable *D* values for the incompatible elements Pd and Au, whereas the parameterization method appears to work well. Modeling results suggest that initial S for this system may have been closer to 2% than 0, but the elements modeled do not tightly constrain initial S.

Consistent with previous studies, our calculated initial concentrations of HSE in the IVB parent body indicate assembly from materials that were fractionated via high temperature condensation processes. As with some previous studies, depletions in redox sensitive elements and corresponding high concentrations of Re, Os and Ir present in all IVB irons are interpreted as meaning that the IVB core formed in an oxidized parent body. The projected initial composition of the IVB system was characterized by sub-chondritic Re/Os and Pt/Os ratios. The cause of this fractionation remains a mystery. Because of the refractory nature of these elements, it is difficult to envision fractionation of these elements (especially Re–Os) resulting from the volatility effects that evidently affected other elements.

* Corresponding author. Fax: +1 3014053597.
E-mail address: rjwalker@geol.umd.edu (R.J. Walker).

0016-7037/$ - see front matter © 2008 Elsevier Ltd. All rights reserved.
doi:10.1016/j.gca.2008.01.021

1. INTRODUCTION

The IVB iron meteorite group currently consists of 12 meteorites. Most previous studies of IVB irons have concluded that they formed as a result of fractional crystallization of a metallic liquid that likely coalesced as an asteroidal core (Schaudy et al., 1972; Rasmussen et al., 1984; Campbell and Humayun, 2005). Tungsten isotope studies have shown that the parental metallic liquids to these meteorites segregated from silicates within several million years of the formation of the solar system (Horan et al., 1998; Scherstén et al., 2006). Crystallization evidently followed soon afterwards. Smoliar et al. (1996) reported a precise ^{187}Re–^{187}Os isochron age of 4527 ± 29 Ma for a suite of 6 IVB irons, indicating early crystallization and subsequent closed-system behavior. Osmium isotopic data presented in Shen et al. (1996) are also consistent with that conclusion.

Compared with other iron meteorite groups, the IVB group is compositionally unusual with high concentrations of Ni (~16–18 wt %) and refractory elements, such as Ir, coupled with low concentrations of volatile elements including Ga and Ge (Fig. 1). Consequently, some previous studies have concluded that the parent body from which the IVB iron meteorites crystallized was distinctly non-chondritic in bulk composition (Kelly and Larimer, 1977; Rasmussen et al., 1984; Campbell and Humayun, 2005). The unusual chemical characteristics of the IVB irons could be the result of nebular fractionation processes (Kelly and Larimer, 1977), processes that may have taken place within the parent body, such as volatile outgassing and/or oxidation (Rasmussen et al., 1984), or a combination of nebular and parent body processes. Most recently, Campbell and Humayun (2005) concluded that no single condensation or heating process could generate the observed volatility relation between the elements present in the projected parental melt to the IVB irons. They proposed a three stage sequence of events to form the IVB parent body that included high temperature nebular condensation, preferential accretion of some refractory-rich components to the parent body, and thermal homogenization and oxidation in the parent body.

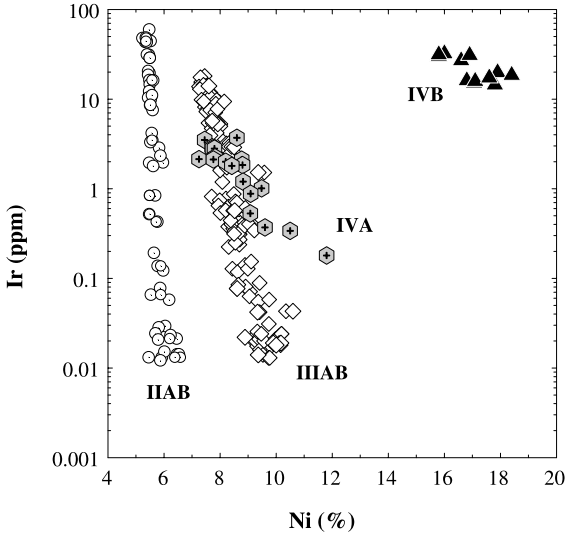

Fig. 1. Nickel (wt.%) versus Ir (μg/g) for magmatic iron groups. Iridum data for IVB irons are from this study and Ni and other Ir data for the IIAB, IIIAB, IVA, IVB irons are from Wasson (1999), Wasson and Richardson (2001), Campbell and Humayun (2005) and Wasson et al. (2007).

Despite the requirement for complex processing to generate the parental melt, the chemical evolution of the IVB system resulting from crystallization of the metallic liquid may be the simplest of the major iron meteorite systems to study. This is, in part, due to low presumed initial concentrations of volatile elements such as S and P, whose presence can lead to complex partitioning behavior of trace elements in metallic systems (Jones and Drake, 1983; Jones and Malvin, 1990; Chabot, 2004). Further, the IVB irons are structurally classified as "ataxites", lacking macroscopic intergrowth of taenite and kamacite. As a consequence of their uniform structure at the macroscopic scale, individual IVB irons are generally chemically homogeneous, and the small pieces that are analyzed for chemical concentrations are unlikely to be substantially biased due to sampling inhomogeneity. The chemical simplicity of the IVB irons, therefore, makes them an appealing target for testing crystal–liquid fractionation models in iron systems.

Here we examine the ^{187}Re–^{187}Os isotopic systematics of the IVB irons and precisely measure highly siderophile element abundances (HSE: Re, Os, Ir, Ru, Pt, Rh, Pd and Au) in bulk samples of each IVB iron. In addition, we re-measure the abundances of these elements and measure 13 additional elements by spot analysis using laser ablation ICP-MS as a means of assessing sample homogeneity and for attempting to further constrain the chemical characteristics of the parental liquid to the IVB irons.

The chief objective of this study is to assess whether a simple fractional crystallization model can account for the variations in the concentrations of each of the HSE among IVB irons. To do this we first examine the ^{187}Re–^{187}Os isotopic systematics of all IVB irons in order to assess whether or not closed-system behavior prevailed following crystallization of each meteorite. Our assumption is that IVB meteorites that plot within uncertainties of a precise, primordial isochron are likely to have had little to no open-system behavior of other HSE subsequent to crystallization. Thus, variations in the concentrations of the HSE among meteorites that are co-isochronous can be attributed solely to primary magmatic processes.

Fractional crystallization of the IVB system is modeled using new HSE data generated for bulk samples of IVB irons. To do this, bulk distribution coefficients or D values (the concentration ratio of the element in the solid metal to liquid metal) were estimated by two methods. One is to use the parameterization method of Chabot and Jones (2003) to calculate D values appropriate for most of the HSE as functions of estimated changes in S and P content. The parameterization provides mathematical expressions for changes in the D values for some HSE as functions of changes in S, P and C (C is not considered here) concentrations, that are consistent with experimental observations. Details of the parameterization used for each element are

provided in the associated Electronic annex. A second, related method is to establish the initial D value of one of the HSE (we use Ir) and calculate relative D values for the other HSE utilizing the slopes of the element pairs on logarithmic plots. As with the first method, changes in D value for the reference element are calculated as per changes in S and P concentrations using the parameterization of Chabot and Jones (2003). The slope-based method is necessary for those elements for which the parameterization has not yet been devised, due to the paucity of experimental data (Ru and Rh). It will be shown that it is also necessary for modeling element pairs, such as Re and Os, with very similar partitioning characteristics. Our modeling approach here differs from previous studies of crystal–liquid fractionation in IVB irons (e.g., Campbell and Humayun, 2005) in that we consider the effects of changing D values on crystallization paths. Further, our approach is one of forward modeling, where D values are independently (parameterization) or semi-independently (slope-based) established, followed by fractional crystallization calculations. In contrast, Campbell and Humayun (2005) used a reverse modeling in which they established D values and percentages of crystallization via a best fit of eighteen elements simultaneously to the meteorite data. Thus, we model a more limited suite of elements but subject the data for individual meteorites to closer scrutiny regarding the fit of each element to a model.

Questions to be addressed via modeling include: (1) Can a simple crystal–liquid fractionation model account for the concentrations of the HSE in the IVB system? (2) Is one method for estimating D values better than another? (3) Can successful models for crystallization be used to constrain proportions of liquid and solid fractions represented in individual meteorites? (4) Can highly precise data be used to better constrain the concentrations of S and P present in the initial liquid than has been accomplished before?

2. ANALYTICAL METHODS

Sawn chunks of all twelve known IVB iron meteorites were obtained from: the Smithsonian Institution National Museum of Natural History (Warburton Range, USNM 985; Tawallah Valley, USNM 1458; Weaver Mountains, USNM 3145; Hoba, USNM 6506; Tlacotepec, USNM 872; Cape of Good Hope, USNM 985; Iquique, USNM 1230; Skookum, USNM 536; Santa Clara, USNM 7191), the Museum for Naturkunde, Berlin (Ternera), the Harvard Peabody Museum collection (Kokomo sample analyzed by isotope dilution), the American Museum of Natural History (Kokomo sample AMNH 48; used for standard addition and laser ablation analysis), and Arizona State University Center for Meteorite Studies (Tinnie, ASU1473).

Iron meteorite samples were cut into 0.05–0.3 g pieces using a Leco 'Vari-cut' saw with a 12.7 cm diameter diamond wafering blade and high purity water used as the cooling medium. To avoid cross-contamination between samples, the blade and blade assembly were cleaned with water after each sample was cut, and the cooling water was discarded and replaced. Blades were further cleaned by cutting a piece of carborundum after washing the blade and prior to cutting the next sample. Prior to dissolution, each meteorite piece was mechanically cleaned by polishing with carborundum. A separate piece of carborundum was used for each sample. Polished pieces were examined under a binocular microscope to verify cleanliness and absence of inclusions.

The chemical-separation techniques used in this study for Re–Os isotopic analysis and isotope dilution analysis of Ir, Ru, Pt and Pd have been previously published (Shirey and Walker, 1995; Rehkämper and Halliday, 1997; Cook et al., 2004; Becker et al., 2006). The polished metal, a mixed spike consisting of ^{185}Re and ^{190}Os, a separate mixed spike consisting of ^{191}Ir, ^{99}Ru, ^{194}Pt and ^{105}Pd, approximately 4 g of concentrated HNO_3 and 2 g of concentrated HCl were frozen into quartz or Pyrex™ Carius tubes, sealed and heated at 240 °C for more than 24 h to obtain complete sample-spike equilibration. Osmium was purified using a carbon tetrachloride (CCl_4) solvent extraction technique (Cohen and Waters, 1996) follow by microdistillation purification (Birck et al., 1997). The Os total processing blank was 3 ± 2 pg ($n = 7$) and was inconsequential for all samples.

Rhenium, Ir, Ru, Pt and Pd were separated and purified from the residual acid using anion exchange columns (200–400 mesh) with a resin volume 0.2 ml. The samples were loaded onto columns in 0.8 M HNO_3, then the elements were successively eluted using 12 mL 6 M HNO_3 (Re and Ru), 15 mL concentrated HNO_3 (Ir, Pt) and 15 mL concentrated HCl (Pd). The Re, Ir, Ru, Pt and Pd blanks for this procedure averaged 2 ± 1, 4 ± 1, 9 ± 3, 300 ± 100 and 60 ± 20 pg, respectively ($n = 2$). All analyses are blank corrected. The blanks comprised <1% of the total element analyzed and had negligible impact on analytical uncertainties.

Osmium was analyzed via negative thermal ionization mass spectrometry (Creaser et al., 1991) using procedures previously discussed (Cook et al., 2004). For the levels of Os extracted from the IVB iron meteorites (>20 ng), external reproducibility in the ^{187}Os/^{188}Os ratio was ±0.05% (2σ) or better, based on repeated analyses of comparable quantities of a standard and duplicate analyses. The analytical uncertainties in the measurement of Os concentrations are estimated to be ⩽0.1%.

Rhenium, Ir, Ru, Pt and Pd analyses were conducted using a *Nu Plasma* multi-collector inductively coupled plasma mass spectrometer (MC-ICP-MS) and a *Cetac Aridus*™ desolvating nebulizer. All analyses were accomplished using static, multiple Faraday bucket collection. Salient ratios were measured to better than ±0.1% (2σ). With the exception of Re and Os, all concentration data are estimated to be precise and accurate to better than ±3%, based on repeated measurements of spiked standards. Rhenium uncertainties are estimated to be ⩽0.1%.

The reported ^{187}Re/^{188}Os ratio 2σ uncertainties include the combined uncertainty in the isotopic measurements and blank corrections. Not included is the uncertainty in the calibration of the Os spike, which results from uncertainties in the stoichiometry of the Os standard used for spike calibration (e.g., Morgan et al., 1995; Yin et al., 2001). The Os and Re blank corrections introduced maxi-

mum uncertainties of ±0.02% for all samples. The maximum uncertainties in $^{187}Re/^{188}Os$ were ±0.2% for all samples.

Concentrations of Au and Rh were measured in all 12 IVB iron meteorites by standard addition solution ICP-MS using a *Thermo-Finnigan* Element 2 single collector-ICP-MS. The primary solutions were created by dissolving ~50 mg of iron meteorite in 10 mL of ultra pure *aqua regia* and a drop of concentrated HF. The mixtures were then heated (~120 °C) in sealed Teflon vials for 24 h to ensure complete dissolution. After cooling, the mixtures were subsequently diluted with 90–100 mL of Milli-Q water and weighed to ensure the proper dilution factor.

For the Au measurements, six standard addition solutions of both Hoba and Ternera were created. The first solution contained 2.5 mL of the dissolved meteorite solution, 2.5 mL ultra pure 2% HNO_3, and 0.25 mL of a 10 ng/g Yb solution in 2% HNO_3 (as a drift monitor); the next 5 solutions included additional increments of 0.05 mL of a 1 ng/g Au, Pd, Pt, Ir, Rh, Ru solution, with the final volume kept constant. Ultimately, multiple standard addition curves of <1–50 pg/g, with increments of ~10 pg/g, were constructed for these analyses. For the rest of the meteorites, one sample solution was created using 2.5 mL of each meteorite solution, 2.5 mL 2% HNO_3, and 0.25 mL 10 ng/g Yb. Rhodium measurements were done in a manner similar to Au using additional solutions of Hoba and Cape of Good Hope. Standard addition curves of <1 ng/g to 5 ng/g with increments of ~1 ng/g were constructed. Following the Yb drift correction, the concentrations of Au and Rh in each meteorite were determined using the standard addition calibration curves for the respective element. Uncertainties in the measured values were calculated on the repeat analyses from multiple experiments and are estimated to be about 5%.

In situ chemical analyses of each sample were carried out using a *Thermo-Finnigan* Element 2 coupled to a laser ablation system with a photon wavelength of 213 nm (UP213, New Wave Research). The mass spectrometer was operated in a dynamic peak hopping mode with mass/charge positioning achieved by a combination of magnet current shifts and voltage offsets (Hamester et al., 1999). The laser ablation system operated in aperture imaging mode using a monochromatic beam at 213 nm, which is generated from a frequency quintupled, solid state Nd-YAG source. This beam was focused on to a sample in a 3 cm^3 ablation cell, which was continuously flushed to the plasma with ~1.1 L/min He gas. Each sample was analyzed under two separate methods that involved different laser and mass spectrometer operating conditions. In the first sequence the laser sampling involved the analyses of four separate, adjacent line traces (~0.8 mm long) produced using a ~100 μm diameter beam. This beam was flashed on to the sample at 7–10 Hz while the sample was moved horizontally at a rate of 10–40 μm/s. Under these conditions the mass spectrometer collected data for the following mass stations: ^{51}V, ^{53}Cr, ^{55}Mn, ^{63}Cu, ^{65}Cu, ^{66}Zn, ^{67}Zn, ^{69}Ga, ^{71}Ga, ^{73}Ge, ^{74}Ge, ^{75}As, ^{95}Mo, ^{97}Mo, ^{99}Ru, ^{101}Ru, ^{103}Rh, ^{105}Pd, ^{108}Pd, ^{182}W, ^{183}W, ^{185}Re, ^{188}Os, ^{189}Os, ^{191}Ir, ^{193}Ir, ^{194}Pt, ^{195}Pt and ^{197}Au. The second sequence, optimized for examining P heterogeneities, involved laser sampling *4* separate, adjacent line traces (~0.5 mm long) that used either an 8 or 15 μm diameter laser beam, flashed at 6 Hz while the sample was moved horizontally at a rate of 10 μm/s. During this sequence the mass spectrometer collected data for ^{31}P, ^{59}Co, ^{61}Ni, ^{63}Cu and ^{65}Cu. Thus, Cu is a shared element between both sequences and provides a cross-check for relative accuracy between sequences. Reported Cu concentrations are for the Cu data collected in the long element menu sequence where we used a larger spot size during ablation. The P, Co and Ni data were determined using a 3-way calibration involving Cu data from the longer menu and Ni and Co data from Rasmussen et al. (1984). For both methods the laser was operated with a uniform energy density of ~2.6 J/cm^2.

Each analysis sequence consisted of five standard reference materials (SRM) run before and after the data acquisition of three separate IVB samples (see Electronic annex for data for these SRMs). Analyses of these SRMs provided multi-sample calibration curves used for determining element concentrations and for constraining instrument drift. All data were processed using the LAMTRACE (Achterbergh et al., 2001) software, which determines element concentrations based on ratios of background-subtracted count rates for samples and standards, known concentrations in the standards and the known concentration of an internal standard in the unknowns. In all cases, the internal standard for the IVB analyses was Pt, as determined by isotope dilution, and was used as an input for ^{194}Pt. Initial compositional analyses involved using each of the following as standard reference materials: Hoba, Coahuila and Filomena for ^{194}Pt (cross-check with input at ^{195}Pt), Ir, Os, Re, W, Pd, Ru, Mo, As and Cu, Hoba for Rh, Au, Ge, Ga, Zn, and NIST 1263a and NIST 1158 for P, Co, Ni and Cu. The assumed concentrations of Au and Rh in Hoba are 0.064 and 3.54 ng/g, respectively, based on the standard addition analysis. The detection limits used in this study were set at the background count rate plus 3 times the standard deviation of the background. Much of the data for Ge and Zn were at or below this limit of detection. The reproducibility reported for individual samples is the standard deviation for the multiple line analyses. For many elements (e.g., HSE) the standard deviation reflects reproducibility at or near counting statistics limit, while for other elements (e.g., P and Cu) this number reflects spatial heterogeneities. Where multiple isotopes of a given element were determined, average concentrations are reported.

3. RESULTS

3.1. Reproducibility and comparison of data with published results

Isotopic and bulk HSE concentration data for the IVB iron meteorites are summarized in Table 1. Duplicate isotope dilution analyses of separate meteorite chunks generally provide identical Re/Os ratios and Os isotopic compositions, within analytical uncertainties. Absolute concentrations of Re and Os in duplicates vary <±1%, with the exception of duplicate analyses of Skookum, which dif-

Table 1
Osmium isotopic and HSE composition data for IVB irons

Sample	Wt.	Ni	Re	Os	Ir	Ru	Pt	Rh	Pd	Au	$^{187}Re/^{188}Os$	$^{187}Os/^{188}Os$	Δ
Cape of Good Hope	0.059	16.3	3249.5	48367	30850	30700	30030	3500	5378	44.0	0.32351(65)	0.12092(6)	−0.3
Duplicate	0.080		3224.3	48152	31910	30390	31190		5234		0.32235(64)	0.12102(12)	1.5
Iquique	0.063	16.0	3243.1	48131	32190	30610	31150	3410	5287	49.3	0.32436(65)	0.12100(6)	−0.3
Kokomo	0.082	15.8	3144.1	46745	31370	30090	31190	3690	5514	58.0	0.32379(65)	0.12101(6)	0.3
Tlacotepec	0.077	15.8	3155.3	46891	30170	30460	30130	3430	5692	50.5	0.32404(65)	0.12095(6)	−0.5
Duplicate	0.068		3139.3	46742	29930	30000	29690		5679		0.32367(65)	0.12096(6)	−0.1
Duplicate	0.060		3135.7	46676	32110	30100	31260		5625		0.32340(65)	0.12096(6)	0.1
Hoba	0.069	16.6	2731.6	39206	26860	29440	30140	3540	6244	64.1	0.33552(67)	0.12188(6)	−0.3
Duplicate	0.053		2729.8	39229	28280	28860	31420		6152		0.33502(67)	0.12188(6)	0.1
Santa Clara	0.089	17.9	1808.8	23517	19790	25650	32320	3860	8055	90.7	0.37044(74)	0.12470(6)	0.2
Tinnie	0.108	18.4	1654.5	20574	18490	26660	31860	3730	10320	133	0.38730(77)	0.12597(6)	−0.4
Ternera	0.074	17.6	1509.7	19271	17280	23930	32430	3960	9567	130	0.37734(75)	0.12525(6)	0.2
Weaver Mtns.	0.084	16.8	1468.6	18203	16110	24890	31330	3610	8974	95.0	0.38875(78)	0.12607(6)	−0.6
Duplicate	0.078		1475.6	18361	16940	24210	32620		8837		0.38714(77)	0.12609(6)	0.8
Tawallah Valley	0.065	17.1	1377.7	16786	15180	23820	31240	3530	9751	152	0.39546(79)	0.12656(13)	−1.0
Duplicate	0.053		1372.6	16777	15580	23570	32680		9691		0.39413(79)	0.12656(6)	0.0
Skookum	0.073	17.1	1356.2	16751	15810	23920	30830	3760	9428	105	0.39023(78)	0.12620(6)	−0.5
Duplicate	0.050		1450.6	17930	16810	24050	32500		9411		0.38973(78)	0.12620(6)	−0.1
Warburton Range	0.097	17.8	1291.0	15630	14430	23450	31370	3750	10250	111	0.39803(80)	0.12701(13)	1.5
Duplicate	0.079		1284.2	15553	14810	23180	32750		10030		0.39776(80)	0.12682(6)	−0.2

Samples are listed in order of descending Re concentration.
Units of weight are in g. Nickel concentrations are given in wt.%. All other concentrations are in ng/g. Nickel data for bulk samples are compiled from Wasson (1974), Buchwald (1975) and Rasmussen et al. (1984). Rhodium and Au were measured by standard addition ICP-MS, remaining elements measured by isotope dilution. 2σ uncertainties listed in parentheses are for last significant figures. Δ is the deviation of $^{187}Os/^{188}Os$ of a sample datum from the IVB isochron in units of per mil, with an uncertainty of ±1 per mil (Cook et al., 2004).

fer by nearly 7%. These results are indicative of minimal to minor heterogeneities with respect to Re and Os within bulk samples on the mm scale sampled by different chunks. Heterogeneities resulting from the sampling of widely separated chunks of the meteorite (e.g., pieces from different museum collections) are not assessed here.

Rhenium and Os concentrations obtained by isotope dilution of bulk samples here are within ~1%, and $^{187}Os/^{188}Os$ ratios are within ~±0.1% of values reported by Smoliar et al. (1996). The similarity is not surprising given that the analyses were done using the same spikes and nearly identical mass spectrometric techniques. Our new Re and Os concentration data are ~2–4% lower compared to the data for the three IVB irons analyzed by Shen et al. (1996). Rhenium and Os concentration data for Tlacotepec are ~2 and 20% lower, respectively, than data reported by Luck and Allègre (1983). Rhenium and Os concentrations are also 7–20% lower than data acquired by laser ablation ICP-MS spot analysis reported by Campbell and Humayun (2005) and Petaev and Jacobsen (2004). Our Re concentrations range from ~16% lower to ~4% higher than data obtained by neutron activation analysis of bulk samples reported by Rasmussen et al. (1984).

Isotope dilution analyses of Ir, Ru, Pt and Pd for multiple chunks of individual meteorites vary a maximum of ±2.5%, ±1%, ±2.2%, and ±1.2%, respectively, with the exceptions of ±4.5% for triplicate analyses of Ir in Tlacotepec and ±3% for duplicate analyses of Skookum. The isotope dilution data for Ir, Ru, Pt and Pd, and standard addition data for Rh and Au differ variably from published data. Compared to concentrations reported by Rasmussen et al. (1984), our Ir concentrations are generally within ±20%, with no systematic offset. In contrast, our Au concentrations are all lower by ~7% to >80%. As with Re and Os, our concentrations of Ir, Ru, Rh, Pd and Au are between ~5% and 20% lower than reported by Campbell and Humayun (2005) and Petaev and Jacobsen (2004), whereas Pt concentrations are within ~3–6%. A comparison of Pd data can also be made with isotope dilution data produced for 6 IVB irons reported by Chen and Wasserburg (1996). Our data are ~7–11% lower than previously reported. Differences between our laser ablation data and literature data are discussed in the Electronic annex.

The causes of the differences are not clear. The results of Rasmussen et al. (1984), and our own data for duplicate samples of Skookum, suggest the possibility of heterogeneities at the 5–30% level for some elements among sample chunks, and in particular, among chunks from different masses of the same meteorite (e.g. samples from different museum specimens). Hence, some of the differences in concentration may represent real heterogeneities among the different specimens examined. Some of the differences, however, are almost certainly analytical biases. At this time the nature of the biases remain unresolved because there currently exist no appropriate absolute standards for these types of measurements. Although the differences between results for the different studies are beyond stated analytical uncertainties, the differences have minimal impact on subsequent modeling done here.

3.2. Overview of data

The minor fractionation of Re from Os during crystallization of the IVB suite led to a limited range in

$^{187}Re/^{188}Os$ from 0.333 to 0.398, and a corresponding range in $^{187}Os/^{188}Os$ from 0.1210 to 0.1270. A ^{187}Re–^{187}Os isochron regression for the twelve IVB irons (and eight duplicate analyses) gives a slope of 0.07927 ± 0.00062 (2σ) and an initial $^{187}Os/^{188}Os = 0.09531 \pm 0.00022$ using *ISOPLOT* (Ludwig, 2003) (Fig. 2). Application of a λ for $^{187}Re = 1.666 \times 10^{-11}yr^{-1}$ (Smoliar et al., 1996) yields an age of 4579 ± 34 Ma (MSWD = 1.3). Precision is limited by the minimal range in $^{187}Re/^{188}Os$. This age and the intercept are similar to a previously reported Re–Os isochron age of 4527 ± 29 Ma and intercept of 0.09559 ± 19 for IVB iron meteorites (Smoliar et al., 1996). The new isochron age is also similar to the Re–Os ages of other iron groups (Luck et al., 1980; Shen et al., 1996; Smoliar et al., 1996; Horan et al., 1998; Cook et al., 2004).

For our suite of bulk samples, HSE concentrations vary modestly by less than a factor of ~3 over the entire range of IVB irons. Most noteworthy is the mere 9% total variation in Pt concentration throughout the entire IVB suite (including duplicate analyses). Chondrite normalized HSE patterns, plotted in order of decreasing 50% condensation temperature, form nested patterns (Fig. 3). The IVB pattern shape is distinctive from typical patterns for other magmatic iron groups (Pernicka and Wasson, 1987; Wasson, 1999; Petaev and Jacobsen, 2004).

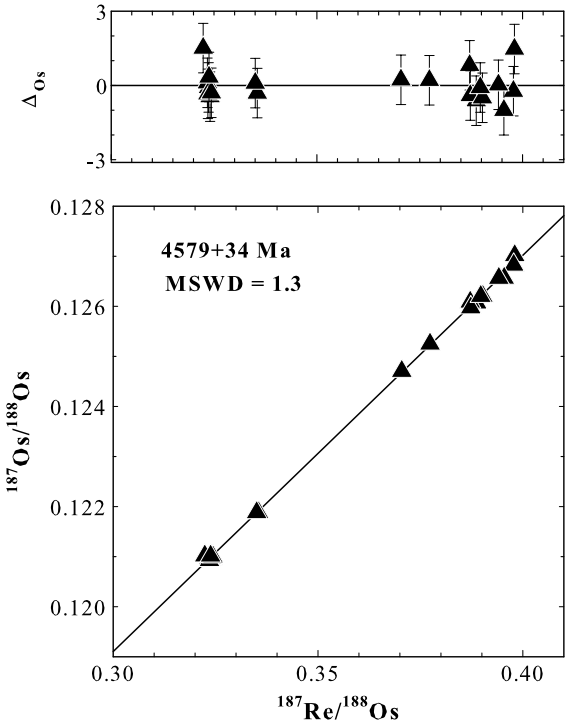

Fig. 2. $^{187}Re/^{188}Os$ versus $^{187}Os/^{188}Os$ for group IVB iron meteorites. Symbol size is larger than analytical uncertainties. Upper diagram shows Δ values versus $^{187}Re/^{188}Os$, calculated relative to the IVB isochron. Error bars represent the total analytical uncertainty (2σ) due to the isotopic measurements and the blank corrections. MSDW is the mean squared weighted deviates, a measure of scatter about the regression.

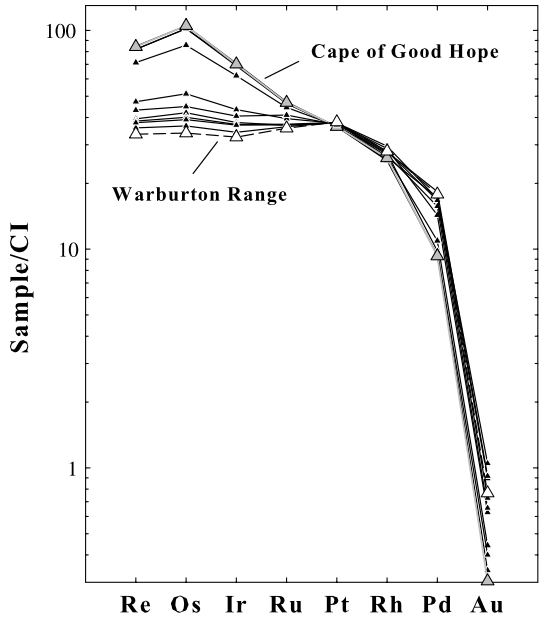

Fig. 3. CI chondrite normalized abundances of HSE for IVB irons. Normalizations achieved using Re, Os, Ir, Ru, Pt, Pd data for the C1 chondrite Orgueil from Horan et al. (2003), Rh and Au data from Anders and Grevesse (1989). For the IVB irons, Ni contents generally increase downward. Cape of Good Hope has the highest Re concentration of this suite and is highlighted with the gray triangles and line. Warburton Range has the lowest Re concentration of this suite and is highlighted with the open triangle symbols and dashed line.

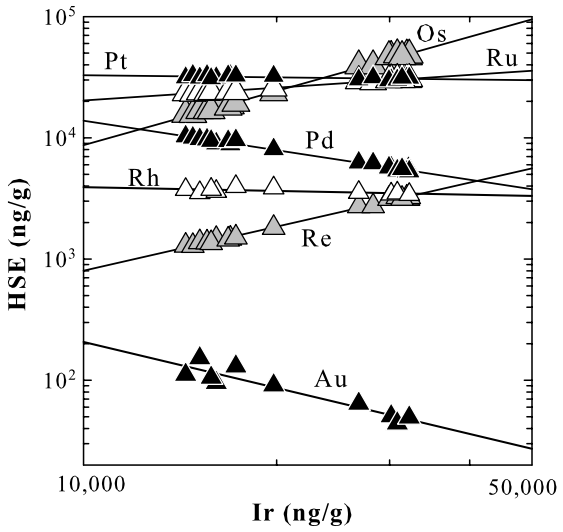

Fig. 4. Logarithmic plot of Ir versus other HSE concentrations. All IVB irons plot along well-correlated linear trends. Results of regressions are provided in Table 2.

Plots of Re, Os, Ru, Pt, Rh, Pd and Au versus Ir for all IVB irons give highly correlated linear trends (Fig. 4). Linear regressions for all IVB data (including duplicate analyses) and associated uncertainties of these trends were calculated using the *ISOPLOT* program (Ludwig, 2003; Table 2).

Table 2
Linear regressions and uncertainties of log–log plots of HSE concentration data vs. Ir

Element	Slope	2σ	MSWD
Re	1.23	0.10	0.17
Os	1.51	0.13	0.15
Ru	0.356	0.076	0.09
Pt	−0.060	0.073	0.22
Rh	−0.11	0.57	0.02
Pd	−0.85	0.09	1.1
Au	−1.28	0.33	0.77

In situ compositional data for the IVB meteorites are reported in Table 3, along with the 1st standard deviations for each element, which are based on the average of multiple line scans. Most differences between HSE data obtained for bulk meteorites by isotope dilution and standard addition versus laser ablation are within analytical uncertainties. Minor differences outside of cited uncertainties likely reflect concentration variations on a micro scale revealed by the *in situ* analyses compared to the averaging achieved by bulk analysis. This conclusion is supported by the minor differences that are also noted for duplicate analysis of bulk samples. Most elements were homogeneously distributed among the different tracks analyzed within the individual meteorite chunks. Laser ablation spectra (i.e. counts/s versus time scans) for some IVB irons, however, show considerable variation in the count rates (e.g., 1–2 orders of magnitude) for P, Cr and Mn. These observations are interpreted as the laser beam sampling phosphides and other phases that are <20 microns across (see the Electronic annex for further details). Fig. 5 is a plot of the averaged element abundances in individual IVB irons normalized to CI carbonaceous chondrites, with element order established by decreasing 50% condensation temperatures from left to right. Comparisons of our new laser ablation data with published data are presented in the Electronic annex.

4. DISCUSSION

4.1. Re–Os isotopic systematics

Although the Re–Os isotopic systematics of the IVB irons do not tightly constrain the age of crystallization, the goodness of fit of the data to a primordial isochron limits possible open-system behavior of Re and Os, and likely the other HSE, to no more than a few tens of Ma subsequent to crystallization. This demonstrates that the HSE abundances of these iron meteorites were set by primary magmatic processes, not later-stage alteration. The initial $^{187}Os/^{188}Os$ ratio for the isochron is similar to estimates for that of the solar system (Smoliar et al., 1996), and so is also consistent with very early crystallization.

4.2. Crystal–liquid fractionation model

Due to the slightly incompatible (favors the liquid) nature of Ni, concentrations of Ni within an iron meteorite group are generally observed to increase with degree of crystal–liquid fractionation (e.g., Scott, 1972; Pernicka and Wasson, 1987; Fleet et al., 1999). For the IVB suite, concentrations of Re, Os, Ir, and Ru generally decrease with increasing Ni (Fig. 1, Tables 1 and 3), indicating that these were compatible trace elements (favor the solid) during crystallization of the IVB system (see also Figure A4 in the Electronic supplement). In contrast, Pd and Au abundances generally increase with increasing Ni, an indication of incompatible trace element behavior. The remarkable lack of variation in Pt concentrations requires a bulk distribution coefficient, or D(Pt) value (ratio of the concentration of Pt in solid to concentration in liquid metal) of ∼unity throughout the crystal–liquid fractionation sequence sampled by the IVB irons. Limited total variation in Rh abundances (17%) indicates behavior similar to Pt. The limited variation in concentration for Pt and Rh are comparable to those reported by Campbell and Humayun (2005). These general correlations between HSE and Ni allow qualitative estimates of partitioning characteristics. Determining precise and accurate D values for the HSE over the course of IVB crystallization, however, is a more difficult task.

The presence of even small quantities of S and P in iron systems generally reduce the tendency of the liquid to host HSE; thus, solid metal–liquid metal D values of HSE tend to increase in systems with increasing S and P (e.g., Jones and Drake, 1983; Jones and Malvin, 1990). Increases in S in the liquid, and to a lesser extent P, are a likely outcome of most crystal–liquid fractionation processes because S and P are highly incompatible elements with solid metal. Combined, these two factors make the HSE in high S and P systems much more complex to model than in low abundance systems (e.g., Cook et al., 2004; Wasson et al., 2007). This problem is exacerbated by the fact that S can leave little direct evidence of its presence in resulting solids, so its abundance in a system is difficult to accurately constrain. Previous studies have concluded that the IVB system crystallized from a liquid with low initial S and P (⩽3 wt.% total) based on the limited presence of sulfides, phosphides and phosphates contained within IVB irons (Buchwald, 1975), and the low P content of the metal (Campbell and Humayun, 2005). This conclusion is also supported indirectly by the evidence for limited fractionation of trace elements such as Au, Ga, Ge and Ir in the IVB suite (Chabot, 2004) and by the fact that IVB irons are strongly depleted in other volatile elements. Thus, the low presumed S and P contents of the IVB system makes it ideal for high precision modeling of HSE in an iron meteorite system.

4.2.1. Partition coefficients

Crystallization of the IVB system is modeled for eight HSE (Re, Os, Ir, Ru, Pt, Rh, Pd and Au) and results are compared with our bulk meteorite data for these elements. The model tested here is based on perfect fractional crystallization of the IVB system (e.g., Scott, 1972). In order to model the HSE in the IVB system, an assumption must be made regarding the initial melt concentration of at least one of the elements. An appropriate initial D value for at least one of the elements (not necessarily the same element) must also be chosen. Further, our modeling was based on the assumption that the D values of HSE in the system

Table 3
In-situ analyses of IVB iron meteorites via laser ablation ICP-MS analyses

	Cape of Good Hope	Iquique	Kokomo	Tlacotepec	Hoba	Santa Clara	Ternera	Weaver Mtns.	Tawallah Valley	Skookum	Warburton Range	Tinnie
P	740 ± 320	500 ± 260	540 ± 21	690 ± 255	550 ± 77	4280 ± 3340	3390 ± 2880	800 ± 760	2220 ± 470	6590 ± 5300	250 ± 20	1300 ± 215
V	0.77 ± 0.08	1.14 ± 0.06	0.47 ± 0.07	0.42 ± 0.02	0.70 ± 0.04	0.18 ± 0.02	*0.046*	*0.13*	0.112 ± 0.007	0.13 ± 0.02	*0.060*	0.10 ± 0.01
Cr	210 ± 6	294 ± 12	170 ± 12	152 ± 3	190 ± 3	100 ± 5	31 ± 4	76 ± 1	67 ± 2	27.4 ± 0.4	35 ± 3	50 ± 4
Mn	2.4 ± 0.1	2.1 ± 0.2	1.4 ± 0.1	2.4 ± 0.1	0.95 ± 0.09	2.9 ± 0.2	0.80 ± 0.07	1.76 ± 0.07	1.49 ± 0.06	1.00 ± 0.02	0.73 ± 0.08	1.08 ± 0.06
Fe%[a]	82.7	83.5	82.6	83.5	83.6	82.3	82.0	81.6	80.8	81.8	82.4	80.8
Co	7650 ± 80	7430 ± 65	7340 ± 85	7585 ± 60	7890 ± 55	7720 ± 75	7870 ± 85	7940 ± 55	7980 ± 65	7590 ± 85	7960 ± 80	8400 ± 110
Ni%	16.5 ± 0.3	15.7 ± 0.2	16.6 ± 0.3	16.3 ± 0.4	16.4 ± 0.2	17.7 ± 0.5	17.2 ± 0.7	17.6 ± 0.4	18.4 ± 0.4	17.4 ± 0.5	16.8 ± 0.6	18.4 ± 0.5
Cu	1.0 ± 0.2	1.30 ± 0.04	6.8 ± 1.8	0.96 ± 0.06	2.2 ± 0.1	1.26 ± 0.07	0.98 ± 0.02	1.0 ± 0.2	1.5 ± 0.2	1.39 ± 0.05	0.97 ± 0.03	1.7 ± 0.2
Zn	0.7 ± 0.2	*0.5*	4.3 ±0.9	0.5 ± 0.1	0.40 ± 0.07	0.37 ± 0.04	*0.2*	*0.2*	*0.4*	0.6 ± 0.1	*0.2*	*0.3*
Ga	0.170 ± 0.014	0.183 ± 0.013	0.222 ± 0.004	0.18 ± 0.02	0.192 ± 0.011	0.230 ± 0.005	0.269 ± 0.008	0.261 ± 0.008	0.267 ± 0.008	0.259 ± 0.015	0.276 ± 0.019	0.242 ± 0.010
Ge	*0.05*	*0.04*	*0.05*	*0.04*	0.05 ± 0.01	*0.05*	*0.02*	*0.03*	*0.03*	*0.04*	*0.03*	*0.04*
As	0.38 ± 0.04	0.42 ± 0.03	0.42 ± 0.02	0.44 ± 0.02	0.48 ± 0.06	0.89 ± 0.03	1.29 ± 0.05	0.94 ± 0.13	1.11 ± 0.04	1.16 ± 0.02	1.31 ± 0.04	0.95 ± 0.09
Mo	22.2 ± 1.1	23.3 ± 0.5	23.8 ± 0.2	23.9 ± 0.5	24.6 ± 0.4	31.0 ± 0.6	34.8 ± 0.6	32.9 ± 0.9	34.4 ± 0.9	32.8 ± 0.7	39 ± 5	33.8 ± 0.8
Ru	29.4 ± 0.3	30.4 ± 0.3	31.7 ± 0.3	29.8 ± 0.3	29.2 ± 0.3	24.9 ± 0.5	24.5 ± 0.3	24.9 ± 0.3	24.0 ± 0.5	23.8 ± 0.3	24.3 ± 0.9	24.4 ± 0.5
Rh	3.44 ± 0.03	3.50 ±0.03	3.50 ± 0.03	3.5 ± 0.1	3.58 ± 0.05	3.65 ± 0.04	3.82 ± 0.07	3.79 ± 0.04	3.70 ± 0.11	3.62 ± 0.07	3.85 ± 0.09	3.95 ± 0.06
Pd	5.23 ± 0.05	5.30 ± 0.05	5.56 ± 0.06	5.72 ± 0.09	6.20 ± 0.06	8.18 ± 0.08	9.9 ± 0.2	9.11 ± 0.09	9.8 ± 0.2	9.2 ± 0.2	10.4 ± 0.4	9.1 ± 0.3
W	2.92 ± 0.06	3.03 ± 0.03	3.08 ± 0.09	3.0 ± 0.1	3.10 ± 0.03	3.09 ± 0.06	2.92 ± 0.03	2.99 ± 0.06	3.01 ± 0.06	2.84 ± 0.09	3.10 ±0.06	3.20 ± 0.03
Re	3.06 ± 0.03	3.21 ± 0.06	3.15 ± 0.16	3.10 ± 0.10	2.73 ± 0.03	1.81 ± 0.05	1.48 ± 0.02	1.40 ± 0.02	1.37 ± 0.03	1.37 ± 0.03	1.23 ± 0.03	1.53 ± 0.03
Os	46.4 ± 0.04	48.8 ±0.05	49.5 ± 0.5	45.9 ± 0.9	39.2 ± 0.4	24.5 ± 0.5	18.7 ± 0.2	17.9 ± 0.2	17.1 ± 0.2	17.0 ± 0.3	15.4 ± 0.2	19.0 ± 0.5
Ir	30.4 ± 0.03	32.1 ± 0.3	31.7 ± 0.3	30.8 ± 0.3	27.6 ± 0.3	20.5 ± 0.3	16.7 ± 0.2	16.5 ± 0.2	15.7 ± 0.2	15.8 ± 0.2	14.7 ± 0.2	17.1 ± 0.4
Pt	30.4 ± 0.06	31.2 ± 0.3	30.9 ± 0.3	30.1 ± 0.3	30.8 ± 0.3	32.5 ± 0.4	31.4 ± 0.3	31.7 ± 0.3	32.0 ± 0.3	30.8 ± 0.3	32.0 ± 0.6	32.6 ± 0.6
Au	0.067 ± 0.002	0.058 ± 0.003	0.130 ± 0.014	0.081 ± 0.011	0.064 ± 0.007	0.138 ± 0.006	0.133 ± 0.005	0.112 ± 0.004	0.148 ± 0.007	0.19 ± 0.02	0.137 ± 0.010	0.163 ± 0.015

Fe and Ni reported in wt%, all other elements are reported in μg/g.

The ±1 standard deviation values reported were determined from the reproducibility of the line analyses, with each sample having a minimum of 3 1-mm long line trace analyses. Data for most of the HSE are at or approaching counting statistics, whereas data for other element, particularly P, reveal gross heterogeneity at the scale of the *in-situ* analyses.

[a] Fe data were determined by difference. Data in italics are estimates, given that these numbers are for signals below the 3 sigma detection limit filter.

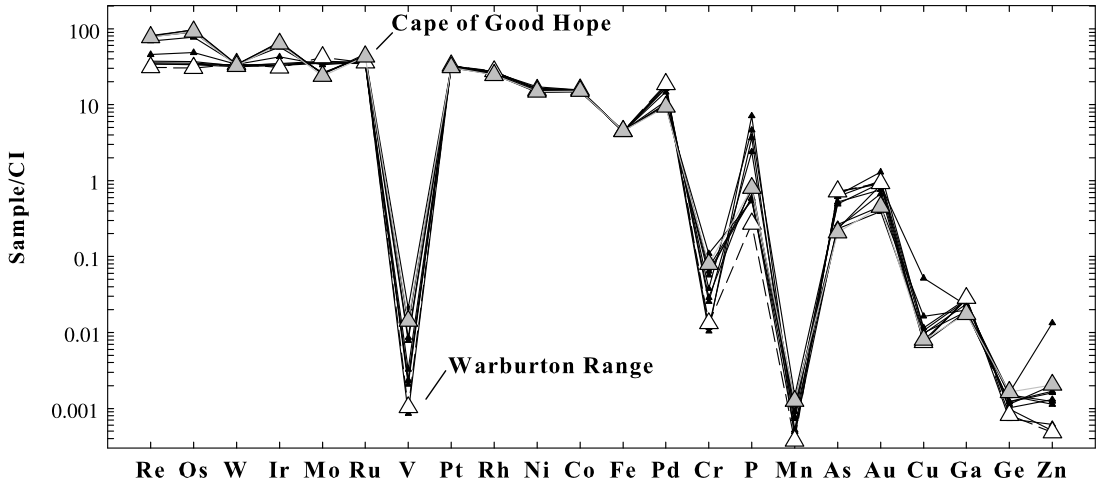

Fig. 5. CI chondrite normalized abundance diagram of elements measured by *in situ* laser ablation analysis. Element condensation temperatures descend from left to right. Note strong depletions in elements sensitive to redox conditions (V, Fe, Cr, Mn, Cu). Gray and open symbols are data for Cape of Good Hope and Warburton Range, as in Fig. 3.

changed as a consequence of increases in S and P concentrations as crystallization proceeded. Thus, some assumptions must also be made regarding how D values change in response to presumed changes in S and P concentrations.

Here we model the fractional crystallization of HSE for a metal system with two starting S and P concentrations. Because Chabot (2004) argued that the collective Au, Ga, Ge, and Ir behavior of the IVB irons is consistent with between 0 and 2 weight % S, we bracketed the model with: (1) an initial parameter having 0.01 wt.% S and 0.70 wt.% P (hereafter referred to as IP1), and (2) an initial parameter having 2 wt. % S and 0.65 wt.% P (hereafter referred to as IP2). In order to model changes in S, a constant D(S) value of 0.001 was assumed throughout the crystallization sequence. As the S content of the model melt increased, concurrent increases in D(P) were calculated using the parameterization of Chabot and Jones (2003). Concentrations of P in the two initial liquids modeled were estimated based on iterative calculations for the two starting S compositions examined and using D(P) values appropriate for the measured P contents of Cape of Good Hope and Iquique. These meteorites have the highest Re concentrations and among the lowest Ni of the IVB irons, so they probably represent early formed solids in the IVB system. The bulk P concentration estimates were obtained by averaging our new data and data from Campbell and Humayun (2005).

There are two approaches that can be taken to estimate changing D values for the HSE. Each has advantages and disadvantages that will be explored. One approach is to use D values calculated for each increment of fractional crystallization and appropriate S and P concentrations using the parameterization method of Chabot and Jones (2003). We did this, where possible, for each element and calculated 0–80% fractional crystallization over 800 increments. This approach is not yet possible for Ru or Rh because of the paucity of partitioning data for these elements in experimental systems over a range of S and P concentrations.

A second, related approach makes use of the fact that *relative* solid metal–liquid metal partitioning characteristics of HSE can potentially be established for natural systems where linear trends on logarithmic plots of the HSE are observed (Morgan et al., 1995; Cook et al., 2004). This allows internally consistent predictions of compositional trends and ratio changes for these elements. As a starting point for modeling, we used an initial D(Ir) value appropriate to the two starting S and P concentrations considered here (Chabot and Jones, 2003), and tracked changes in D(Ir) resulting from crystal–liquid fractionation and the accompanying increases in the S and P contents of the liquid using the parameterization of Chabot and Jones (2003). Iridium was chosen as the "anchor" HSE because its solid metal–liquid metal partitioning is the best experimentally constrained of the HSE. For plots of log[Ir] versus log[HSE]:

$$\text{Slope of correlation} = [D(\text{HSE}) - 1]/[D(\text{Ir}) - 1] \quad (1)$$

Because the logarithmic plots of Ir versus Re, Os, Ru, Pt, Rh, Pd and Au for all IVB irons define highly-correlated linear trends (Fig. 4; Table 2), the slopes, combined with Eq. (1), can be used to calculate D values for each HSE over each increment of crystallization, given the appropriate D(Ir). The fundamental assumption being made when using slopes to calculate relative D values is that all of the changes in D values among the elements modeled are co-linear throughout crystallization, even as the absolute D values change. If this assumption is not met, the D value calculated using Eq. (1) yields inappropriate partitioning values. For this approach it is also assumed that the slopes are defined primarily by meteorites that represent solids crystallized from the primary melt, not samples influenced by trapped liquids. In the case of the IVB iron system, the inclusion of some meteorites with compositions resulting from >50% trapped liquids would not greatly affect the calculated slopes because of the relatively limited presumed differences between solid and liquid concentrations of most HSE in low S and P systems.

4.2.2. Estimation of initial liquid concentrations

Initial concentrations of HSE for the two sets of starting parameters and *D* values modeled here were chosen via a selection of first Re, then Os, followed by Pt and other HSE concentrations. Rhenium and Os were used to define starting concentrations because they are the best measured of the HSE and because their isochronous relation in IVB irons indicates they were unaffected by possible secondary processes. Further, the ratio constraints for chondrites are best defined for Re/Os and Pt/Os compared to ratios of other HSE because of the sensitivity of $^{187}Os/^{188}Os$ and $^{186}Os/^{188}Os$ ratios in modern chondrites to track these ratios over the history of the solar system (Walker et al., 2002). The isotopic parameters $^{187}Re/^{188}Os$ and $^{190}Pt/^{188}Os$ range from ~0.39 to 0.44 and 0.0017 to 0.0020 in bulk chondritic meteorites, respectively, with few exceptions (Walker et al., 1997; Walker et al., 2002; Brandon et al., 2006). Corresponding elemental ratios for Re/Os and Pt/Os range from 0.082 to 0.092 and 1.7 to 2.0, respectively.

Solid metal–liquid metal *D* values for Re (and Os) are ~2 for low S + P systems (<3 wt.%)(Chabot and Jones, 2003). Consequently, if the highest Re, lowest Re/Os IVB irons, Cape of Good Hope and Iquique, are representative of early formed solids in the IVB system, the initial Re concentration of the liquid must have been quite high, given that these irons contain ~3200 ng/g Re. For IP1 and IP2 we minimized initial liquid Re concentrations, but concentrations ⩾1600 ng/g are required for all sets of initial parameters. Such concentrations may be considered high because metal cores segregating from a chondritic precursor would normally have HSE concentrations no more than factors of 3–5 times bulk chondrites (e.g., approximately 500 ng/g for Re; 5 times that of one of the highest Re contents of 100 ng/g in bulk chondrites; Walker et al., 2002), if the parent body cores comprise 20–30% of the mass of the body. For this assumption, the initial IVB liquid would have to have been enriched by at least a factor of 3 relative to the expectation for metal segregated from a chondritic precursor. An alternate interpretation of the high HSE concentrations is that the proportion of segregated metal in the IVB parent body was much less than 20% of the mass of the body (Petaev and Jacobsen, 2004). This could be envisioned for an oxidized parent body within which much of the iron is retained in silicates, and is consistent with the high Ni content of IVB irons.

For IP1 and IP2 the initial Re concentrations chosen generate early (within the first 20% of fractional crystallization) solids with concentrations similar to those present in Cape of Good Hope and Iquique. From this, Os concentrations are constrained by Re/Os ratios to be as close to the range defined by chondrites as possible, such that early crystallization would again produce solids with compositions similar to Cape of Good Hope and Iquique. Most asteroidal cores (e.g., the initial melt) likely had Re/Os (and Pt/Os) within the range of bulk chondritic meteorites (Cook et al., 2004). This is because of the normal presumption of a parent body with chondritic Re/Os (and Pt/Os) coupled with the expectation that metal segregation effectively extracts most of the HSE from the silicate portion of the body, regardless of the proportion of metal. It has been argued that the parent body of the IVB core had non-chondritic relative abundances of most elements (Schaudy et al., 1972; Kelly and Larimer, 1977; Campbell and Humayun, 2005). Our modeling, below, confirms this conclusion for the HSE. Nevertheless, Re and Os, and to a lesser extent Pt, are difficult to substantially fractionate by volatilization/condensation processes, or plausible redox effects, so although the evidence is strong that the parent body of the IVB irons contained fractionated abundances of the HSE, we chose initial parameters for HSE ratios to be as similar to those in chondrites as the model permits.

Once initial Os concentrations were established, Pt concentrations were chosen to provide Pt/Os ratios in early solids to be similar to those of Cape of Good Hope and Iquique. The initial concentrations of the remaining HSE were then established using appropriate *D* values (obtained by both parameterization models and slope-based calculations, where possible) to calculate initial liquid concentrations that would lead to the crystallization of equilibrium solids that are slightly less evolved than Cape of Good Hope and Iquique.

To summarize our procedural plan we: (1) assume two bracketing compositions for S and P in the initial IVB liquid that span the range of previous estimates, (2) computationally allow these compositions to fractionally crystallize and monitor changes in S and P, (3) calculate changing *D*(Ir) values (and *D* values for other HSE where possible) with changing S and P compositions, (4) as a second means of obtaining *D* values for HSE, insert the *D*(Ir) values into Eq. (1) along with the slopes of linear correlations between Ir and other HSE, (5) calculate element versus element fractionation trends for solids and liquids and compare these trends to the data for IVB irons.

4.2.3. Re–Os elemental systematics

Meteorites formed via fractional crystallization of a metallic core can represent a solid directly precipitated from a liquid with which it was in equilibrium, a liquid composition that may be preserved via entrapment within earlier formed solids, or equilibrium melt trapped within and mixed with coexisting solids (Wasson, 1999). In these cases, a meteorite will have a bulk composition that plots along a calculated "solid track", representing equilibrium solids, along a "liquid track", or if a mixture of equilibrium solid and liquid, between the solid and liquid tracks (Cook et al., 2004; Wasson et al., 2007).

We first consider fractional crystallization of the IVB system with respect to a plot of Re versus Re/Os. A meteorite representing a mixture of equilibrium solids and trapped coexisting liquids will plot between the liquid and solid tracks along mixing lines calculated for different extents of crystal–liquid fractionation. A plot of these elements has the disadvantage of incorporating two similarly compatible elements in metallic systems. Thus, it is not ideal for assessing the proportion of trapped equilibrium liquids versus equilibrium solids in individual meteorite bulk compositions. However, as noted above, this element pair is appropriate for establishing initial concentrations of the HSE for modeling. In addition, because of the similarity in partitioning of the two elements, relative *D* values

Table 4
Bulk distribution coefficients (D values) for modeling fractional crystallization using the two sets of initial parameters (IP1 and IP2) discussed in the text

	$IP1_I$	$IP1_{80}$	$IP2_I$	$IP2_{80}$
$Ir_{C\&J}$	1.60	2.07	1.91	7.19
$Re_{C\&J}$	2.14	2.79	2.56	9.89
Re	1.74	2.31	2.12	8.60
$Os_{C\&J}$	2.14	2.79	2.6	10.2
Os	1.90	2.61	2.38	10.3
Ru	1.21	1.38	1.32	3.20
$Pt_{C\&J}$	0.858	1.08	1.01	3.31
Pt	0.964	0.936	0.945	0.629
Rh	0.940	0.893	0.900	0.320
$Pd_{C\&J}$	0.436	0.462	0.454	0.611
Pd	0.506	0.120	0.249	−4.09
$Au_{C\&J}$	0.257	0.285	0.276	0.474
Au	0.232	−0.368	−0.168	−6.92
$Ni_{C\&J}$	0.867	0.895	0.886	1.04

I and 80 subscripts refer to values calculated for the inception of crystallization and after 80% crystallization. C&J—derived from Chabot and Jones (2003) parameterization. Other values obtained from slopes relative to Ir (Table 2).

calculated by the slope method are little biased by meteorites that incorporated variable proportions of trapped equilibrium liquids, as might happen with elements with much more disparate partitioning characteristics. Further, as noted above, the Re–Os element pair constitutes the most precisely measured of the HSE.

The extents of changing D values for each element as calculated using both the Chabot and Jones (2003) parameterization and the slope based methodology are provided in Table 4. A problem with the application of the Chabot and Jones (2003) parameterization method to characterize relative D values for Re and Os is immediately apparent. For both IP1 and IP2, these elements have identical D values for all S and P contents, resulting in no change in Re/Os with extent of fractional crystallization. Yet the IVB irons are characterized by modest but significant variations in Re/Os, so direct application of the parameterization method to modeling Re and Os for this system fails. The reason for the failure is due to the relatively similar D values of Re and Os. Given the precision of the experimental studies, the experimental studies can not resolve slight variations in the partitioning values of these elements. Despite the failure of the parameterization for this element pair, we calculated appropriate initial Re and Os concentrations based on starting D values, so that initial concentrations of the other HSE could be calculated as discussed above (Table 5).

An acceptable match to all IVB meteorite data can be obtained using D values for Re and Os that are determined from the slopes of the trends of these elements versus Ir (Fig. 6a–b). The "liquid track" shows the path of liquid evolution resulting from fractional crystallization of the initial liquid, and the path of accompanying solids are shown as the "solid track". Mixing curves between equilibrium solids and liquids are shown for 20% increments of crystallization. The fractional crystallization model satisfactorily accounts for the data for all IVB iron meteorites as primary solids, liquids, or mixtures of solids and equilibrium liquids, using either set of initial parameters. For IP1, irons plotting on or near the solid track could be representative of equilibrium solids derived from the evolving liquid following approximately 15% (Cape of Good Hope and Iquique) to ~70% (Tinnie) fractional crystallization. The more evolved, lower-Re irons that plot between the solid and liquid tracks would represent mixtures of equilibrium solids and trapped liquids formed after ~50–75% fractional crystallization. For IP1, only Ternera plots on the liquid track. It would represent a nearly equilibrium liquid composition after approximately 37% fractional crystallization. We will track Tinnie, Ternera and Santa Clara, in subsequent plots to assess consistency.

For fractional crystallization using IP2, the liquid and solid tracks are separated more than for IP1 because of the greater difference between initial D values for Re and Os. The solid track also has a steeper slope, and the more evolved, lower Re meteorites plot further to the left of the solid track. Only the meteorites with the highest Re concentrations could be representative of equilibrium solids. The remaining samples, including Tinnie and Ternera, would have formed as mixtures of variable proportions of equilibrium solid and liquid.

Fractional crystallization for each of the two sets of initial parameters requires the Re/Os ratio of the initial liquid to be <0.73, substantially below the normal range of bulk chondrites (Fig. 6a).

4.2.4. Pt–Os elemental systematics

The modeling of fractional crystallization for IP1 and IP2 applied to Pt–Os concentration systematics provides similar insights to Re–Os (Fig. 7a–d). As noted above, a remarkable aspect of the IVB irons is the very limited variation in Pt concentration. Consequently, the Pt axes in plots of Pt versus Pt/Os are condensed to include only a

Table 5
Calculated initial concentrations for models discussed in text (in ng/g)

	Re	Os	Ir	Ru	Pt	Rh	Pd	Au
$IP1_{C\&J}$	1700	25500	21000	N/A	35000	N/A	11300	165
IP1	2100	29000	21800	26500	31800	3720	N/A	N/A
$IP2_{C\&J}$	1410	21600	17500	N/A	29800	N/A	10900	153
IP2	1710	23400	17500	23800	32200	3890	N/A	N/A
C& H	2800	37000	27000	27400	29500	4960	8600	130

C&J—calculated using parameterization of Chabot and Jones (2003). C&H—from Campbell and Humayun (2005). N/A—not applicable for reasons discussed in text.

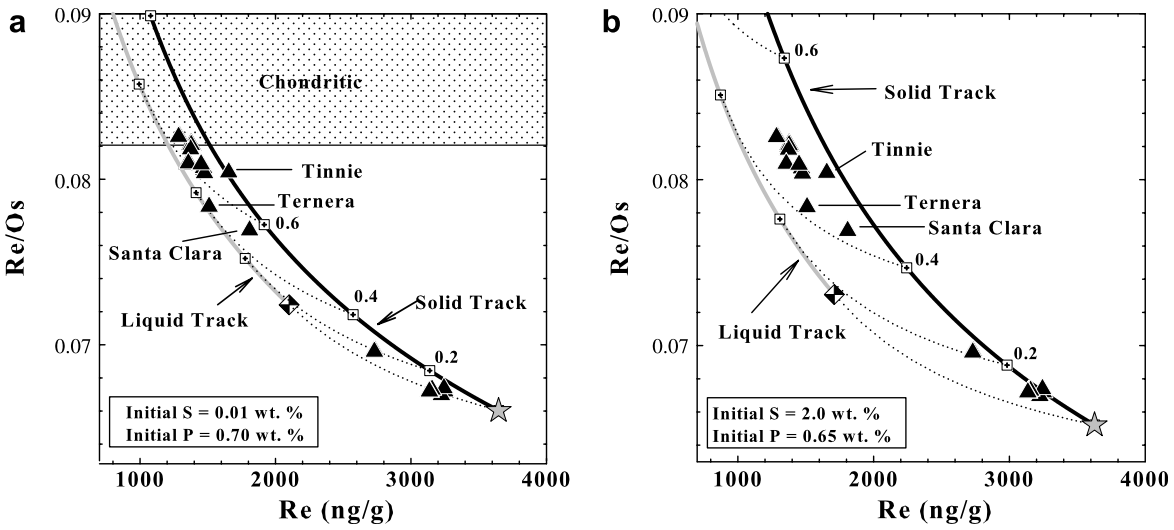

Fig. 6a–b. Fractional crystallization model for Re (in ng/g) versus Re/Os calculated for two pairs of initial parameters (IP1 and IP2), which define the S and P concentrations assumed for the model. D(Re) and D(Os) were determined via the slope method discussed in the text. The method used to select the initial parameters is also discussed in the text. The black triangles are the data for the IVB irons. Where duplicate analyses were determined, the symbols shown are averages. Shown for comparison are liquid (gray) and solid (black) evolution tracks, as discussed in the text. The partially filled diamond symbol represents the starting liquid composition. The gray star represents the composition of the first solid to form. Open squares with crosses along the liquid and solid tracks correspond to increments of 20% fractional crystallization. Mixing curves (dotted) connect the equilibrium solids and liquids at each of these fractions. The range of Re/Os ratios within which most bulk chondrites plot is shown in the stippled area in (a).

very limited range of Pt concentrations. Fractional crystallization for IP1 and IP2 was first modeled for D values calculated using the parameterization method of Chabot and Jones (2003) (Fig. 7a and b). Initial D(Pt) values for IP1 and IP2 are 0.86 and 1.0, respectively. The parameterization leads to modest increases in D(Pt) values with increasing S + P (Table 4). The parameterization-based results for IP1, however, lead to liquid and solid tracks that plot to the right of most data for IVB meteorites. The model cannot be improved by adjusting initial Pt concentrations, so the meteorites cannot be accounted for by equilibrium mixing processes and this aspect of the model fails. The higher D values for IP2 move the liquid track well to the left of the solid track with the higher Pt meteorites plotting between the liquid and solid tracks after ~35–45% fractional crystallization.

The failure of the parameterized D(Pt) values calculated for IP1 to adequately match the IVB trends may indicate the system began crystallization with higher S, or that there are problems with the parameterized equation for D(Pt). Some amount of scatter is inherent in all experimental data; in the case of D(Pt), the scatter would allow slightly different parameterized fits. For example, Chabot and Jones (2003) chose a value for D(Pt) in the S-free system of 0.81; however, an equally good fit to the experimental data could be obtained with a D(Pt) value for very low S of 0.97. Since the D value for Pt in the low S system is very close to 1, minor changes in its value can produce quite different crystallization trends when modeled. Thus, our modeling results suggest that the D(Pt) parameterization of Chabot and Jones (2003) should be examined in more detail prior to being applied to modeling of very low S and P systems.

The D(Pt) and D(Os) values obtained from their slopes relative to Ir were also used in fractional crystallization calculations (Fig. 7c and d). For IP1, all but one meteorite plots within uncertainties of the solid track, liquid track, or the region between. The average Pt concentration for triplicate analyses of Tlacotepec plots just to the left of the solid track. Using slope derived D values and IP1, Ternera barely overlaps with the liquid track and does not overlap within uncertainties of the solid track. This is consistent with its position on the Re–Os plot. A minor discrepancy between the two sets of elements is that in contrast to the Re–Os plot, where it plots between the solid and liquid tracks, Santa Clara plots along the liquid track for Pt–Os.

For IP2, it is necessary to appeal to equilibrium solid-liquid mixing to account for some of the more fractionated, higher Pt irons, as with Re–Os plot. The percentages of fractional crystallization required to achieve the different meteorite compositions for IP2 using the slope-based D values are similar to those estimated from the Re–Os portion of the model. As with IP1, Santa Clara lies on the liquid track for Pt–Os, but not for Re–Os. With minor exceptions, fractional crystallization for both Re–Os and Pt–Os using IP1 and IP2 and slope-based D values give consistent results. The greater spread between solid and liquid tracks for IP2, however, allows all data, including Tlacotepec, to be captured between solid and liquid tracks, so we consider it a slightly better fit to the data.

One aspect of the modeling that is *not* consistent with our understanding of the effects of increasing S and P on D(Pt) is the slightly *decreasing* D(Pt) values with increasing S + P, which is obtained from the slope-based estimates. Solid metal–liquid metal partitioning experiments show

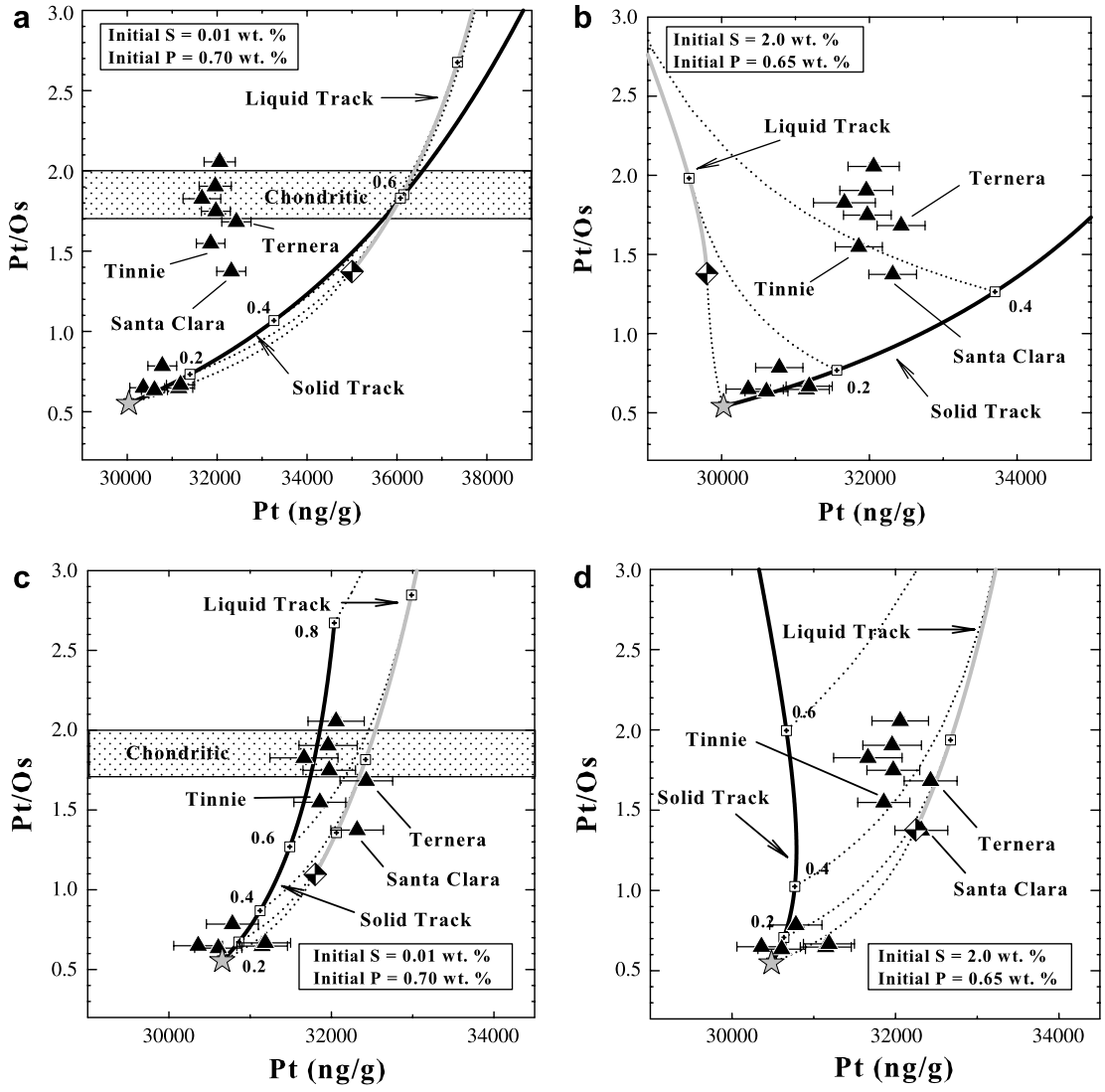

Fig. 7a–d. Fractional crystallization model for Pt (in ng/g) versus Pt/Os calculated for two pairs of initial parameters (IP1 and IP2) which set S and P concentrations. Symbols are the same as for Fig. 6. Error bars represent 2σ analytical uncertainties. (a–b) Fractional crystallization model calculated for two sets of initial parameters using D values calculated using the paramterization of Chabot and Jones (2003). (c–d) Fractional crystallization model calculated for two sets of initial parameters (IP1 and IP2) with D values estimated from slopes of log[Pt] and log[Os] versus log[Ir]. The range of Pt/Os ratios within which most bulk chondrites plot is shown in the stippled areas of (a) and (c).

unequivocally that D(Pt) increases with increasing S and P (Chabot and Jones, 2003). Because of the limited S and P for IP1, the D value for Pt remains essentially constant with changes in S and P having little impact on Pt concentrations (Table 4). This is not so for IP2. However, the unlikely tendency towards decreasing D(Pt) is probably a reflection of the uncertainty in the slope. The Ir–Pt slope for IVB irons overlaps with a slope of zero within uncertainties (i.e., no change in D value relative to a changing D(Ir)), with the uncertainty permitting slightly positive slopes.

Platinum concentrations in bulk chondrites range to as high as ~1800 ng/g (Horan et al., 2003). Using the same reasoning as for Re, the highest Pt content we might expect in a normal core segregated from a chondritic precursor is ~9000 ng/g (1800 × 5). Thus, if the IVB core represented >20% of the mass of the parent body, the initial IVB liquid would have to have been enriched by at least a factor of 3 compared to the expectation for a normal asteroidal core, consistent with our observation for Re. Further, the Pt/Os ratios of bulk chondrites vary from approximately 1.7–2.0 (Walker et al., 1997), yet all of the Pt–Os models require an initial liquid with Pt/Os < 1.5, which is substantially subchondritic and generally consistent with the Re–Os model requirements.

4.2.5. Other HSE

The fit of the IVB iron data to model-generated solid and liquid evolution tracks for the remaining HSE is now considered for IP1 and IP2. Because initial abundances of Re were set first for IP1 and IP2 above, initial abundances of Ir, Ru, Rh, Pd and Au were established relative to Re (Table 5). On plots versus Re, initial abundances of these

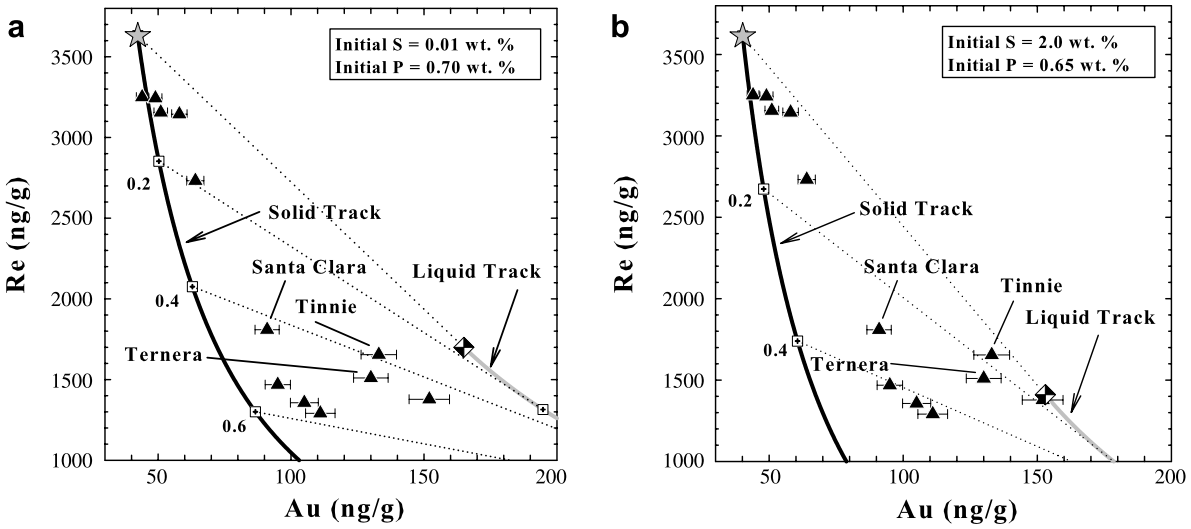

Fig. 8a–b. Fractional crystallization model for Re versus Au calculated for two sets of initial parameters (IP1 and IP2), as discussed in the text. Calculations were made with *D* values determined using the parameterization method of Chabot and Jones (2003), as discussed in the text. Symbols are the same as in Fig. 6.

elements were set so that the data for Cape of Good Hope and Iquique plot along the solid tracks within the first 5–20% crystallization. *D* values for Au, Pd and Ir were first calculated using the Chabot and Jones (2003) parameterization (Table 4).

The large differences in *D* values between Au and Re lead to greater separation between liquid and solid tracks than for Re-Pt–Os plots, and make this element pair potentially more useful for assessing the proportion of liquid to solid metal incorporated into individual iron meteorites. For this task, similar plots of Ir versus Au have previously been used for other iron systems (e.g. Wasson, 1999). Modeling results for the plot of Re versus Au for IP1 and IP2 are acceptable fits to the meteorite data (Fig. 8a–b). All three of the irons tracked in previous plots, Ternera, Santa Clara and Tinnie, along with all other more evolved IVB irons plot between solid and liquid tracks. The plot for IP2 is in general agreement with the complementary plot for Pt–Os, with most meteorites lying roughly in the same locations relative to liquid and solid tracks. Because of the problems raised with the Re–Os plots for IP1 and IP2, and the problem with IP1 for Pt–Os, this is the only direct comparison that can be made to Re–Pt–Os using the *D* values obtained from the Chabot and Jones (2003) parameterization.

The plots of Re–Pd for IP1 and IP2 are very similar to Re-Au with no major discrepancies (Fig. 9a–b). In contrast, plots of Re–Ir for IP1 and IP2 result in the more evolved

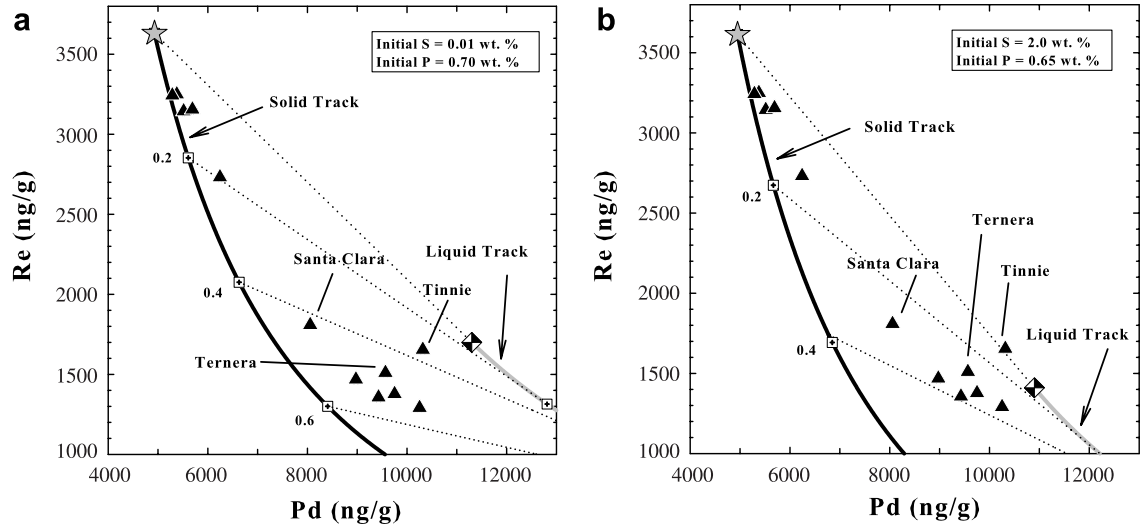

Fig. 9a–b. Fractional crystallization model for Re versus Pd calculated for two sets of initial parameters (IP1 and IP2), as discussed in the text. Calculations were made using *D* values determined using the parameterization method of Chabot and Jones (2003), as discussed in the text. Symbols are the same as in Fig. 6.

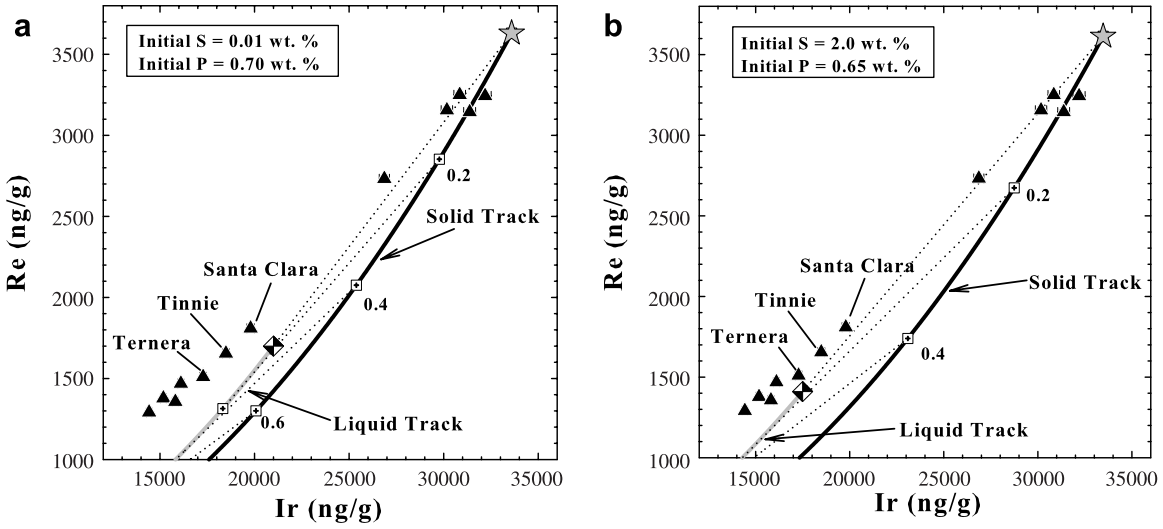

Fig. 10a–b. Fractional crystallization model for Re versus Ir calculated for two sets of initial parameters (IP1 and IP2), as discussed in the text. Calculations were made using D values determined using the parameterization method of Chabot and Jones (2003), as discussed in the text. Symbols are the same as in Fig. 6. Note that the more evolved (lower Re and Ir) meteorites plot to the left of the liquid track, suggesting that the modeling parameters used here are not correct.

IVB irons plotting to the left of the liquid tracks. The model, therefore, does not provide an acceptable fit to the IVB data for either IP1 or IP2 (Fig. 10a–b). Comparison plots for Ru and Rh using D values from the parameterization cannot be made because the parameterization has not yet been extended to these elements.

In order to evaluate the slope-based method to determine relative D values, values for Ru, Rh, Pd and Au were calculated based on their slopes versus Ir (Table 4). Plots of Re versus Ru are consistent with crystallization as equilibrium solids, liquids or mixtures (Fig. 11a–b). The locations of individual meteorites on the plots are generally comparable to the locations on the Re–Pt–Os plots. In order to estimate appropriate initial Ir concentrations for IP1 and IP2, we plotted Re–Ir liquid and solid evolution tracks based on the parameterized values for Ir and the slope-based D values for Re, then fitted the tracks to the meteorite data. We don't consider this plot here because it is based on D values obtained by both methods, and therefore not directly comparable to the other plots. Nonetheless, all IVB data plot between solid and liquid tracks for both IP1 and IP2.

As with Pt, the problem of decreasing D value with increasing degree of crystal–liquid fractionation was manifested in slope-based estimates of D for Rh, Pd and Au, all incompatible elements. This result at least for Pd and Au is inconsistent with experimental observations of increasing D with increasing S and P. Partitioning data for Rh are very sparse, but the limited data also suggest increasing D(Rh)

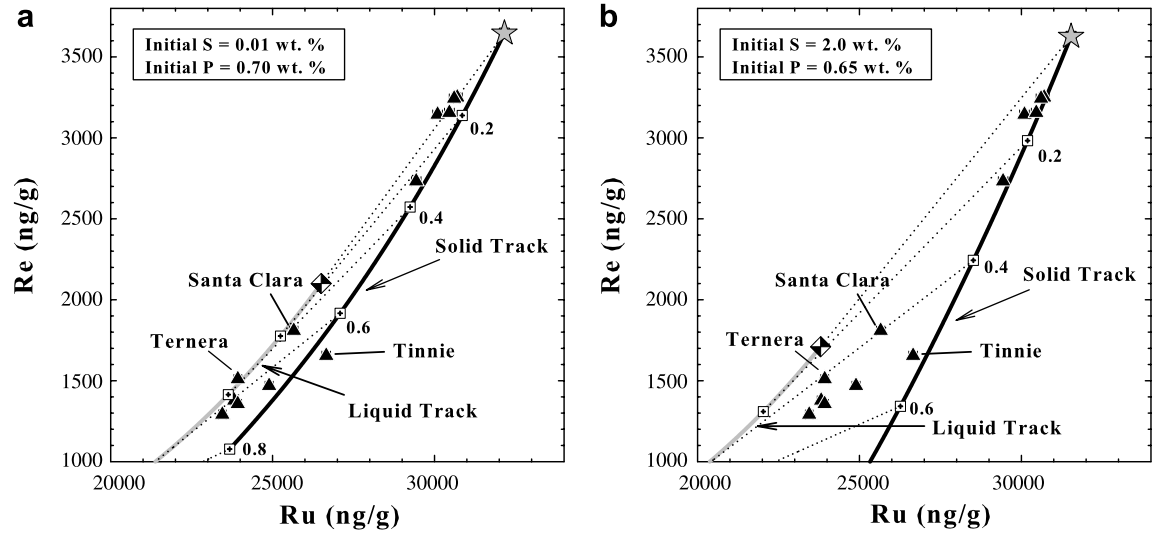

Fig. 11a–b. Fractional crystallization model for Re versus Ru calculated for two sets of initial parameters (IP1 and IP2), as discussed in the text. D values were estimated from slopes of log[Re] and log[Ru] versus log[Ir]. Symbols are the same as in Fig. 6.

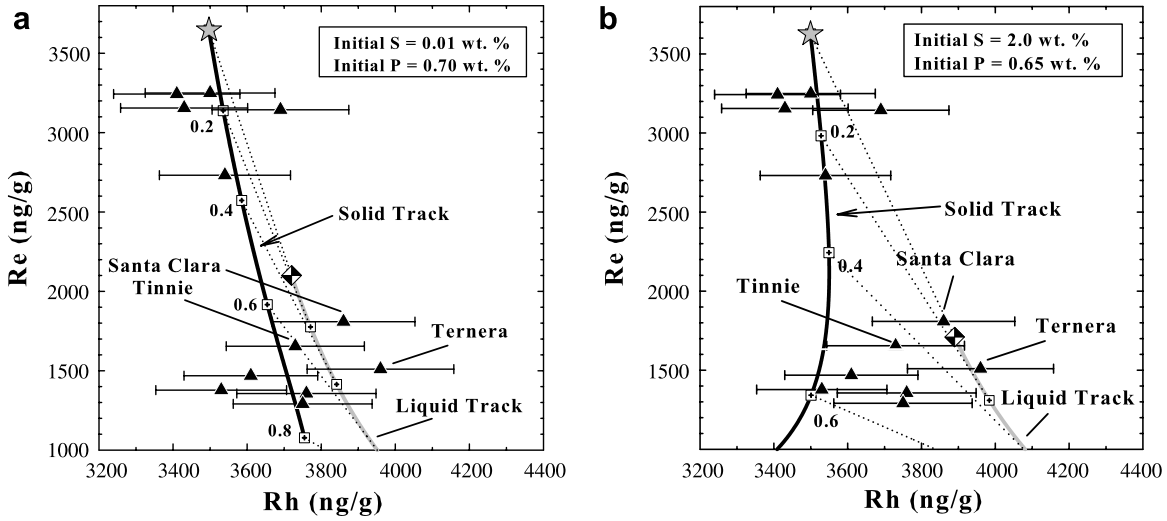

Fig. 12a–b. Fractional crystallization model for Re versus Rh calculated for two sets of initial parameters (IP1 and IP2), as discussed in the text. *D* values were estimated from slopes of log[Re] and log[Rh] versus log[Ir]. Symbols are the same as in Fig. 6.

with increasing S content of the metallic liquid (Fleet and Stone, 1991). Similar to the problem with Pt, the minor trend to negative *D* values can be ameliorated for IP1 or IP2 by revising the slope upward to be slightly positive within regression uncertainties (Table 2). If this is done, plots of Re versus Rh for IP1 and IP2 are consistent with crystallization as equilibrium solids, liquids or mixtures (Fig. 12a–b). The Re–Rh plot, like Pt–Os is not very diagnostic for assessing proportions of solid to liquid because of the limited variation in Rh among the meteorites.

For IP1 and IP2, slope-based *D* values for Au and Pd decrease rapidly with increasing S and P and approach 0 or extend to negative values. The slopes of these elements are negative and are not positive within regression uncertainties (Table 2). The model ultimately fails for both elements when *D* values become negative (mathematically resulting in negative calculated Pd concentrations in precipitating solids!) after ~35–65% fractional crystallization. These results are not realistic and could reflect either a major error in the experimentally derived *D*(Ir), or more likely, some error in the application of the slope-based approach. The most likely culprit is that the plots of log[Ir] versus log[Pd] and log[Au] are not truly linear, so the assumption of *D* values for Pd and Au that change in lockstep with Ir are not correct. This possibility can be illustrated for Au by calculating the solid track on a plot of log[Ir] versus log[Au] using *D* values derived from the parameterization of Chabot and Jones (2003) for both elements. For this case, the resulting curve fits the data as well as the linear regression (Fig. 13).

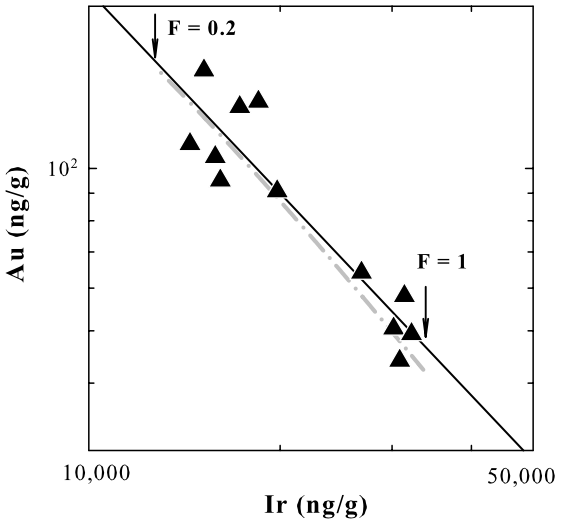

Fig. 13. Logarithmic plot of Ir concentration versus Au for IVB irons. The solid line is the least squares regression of the data. The dash-dotted gray line represents the predicted evolution of equilibrium solids using *D* values obtained using the parameterization of Chabot and Jones (2003). Arrows represent solid compositions for initial solids (100% liquid or $F = 1$) and after 80% crystallization ($F = 0.2$).

4.2.6. Modeling conclusions

A simple, internally consistent fractional crystallization model is capable of accounting for almost all of the HSE concentrations of IVB iron meteorites. Slope-based estimates of *D* values linked to experimentally determined *D*(Ir) work especially well for modeling Re, Os, and acceptably well for Pt, Ru, and Rh. The parameterization methodology of Chabot and Jones (2003) is required for modeling Pd and Au. Only the parameterization of *D*(Pt) for the very low S system IP1 fails to account for the IVB data. Conversely, the slope-based estimates for *D*(Au) and *D*(Pd) fail to reproduce the IVB data, presumably because this *D* value was not changing linearly with Ir as crystallization proceeded. Thus, slope-based estimates of *D* values are probably best used for modeling compatible elements with generally similar partitioning characteristics. The parameterized estimation method is currently best used to model elements with significant differences between their *D* values, as seen in our modeling of incompatible elements.

The fractional crystallization model, for a specified set of initial parameters and using D values obtained by one method or the other, can be used to crudely constrain the proportion of equilibrium solid and liquid present in each meteorite. It does this in a manner that is generally consistent among the different elements studied. For example, the fractional crystallization model for both IP1 and IP2 using slope-based D values indicate that Ternera has a higher proportion of an equilibrium liquid component than the other IVB irons. The liquid–solid proportion estimated for any meteorite, however, *is* dependent on the choice of starting S and P, so modeling cannot provide a unique solution. This aspect of modeling is better for iron groups with higher S and P, because the separation between calculated solid and liquid tracks is much greater (e.g., Wasson et al., 2007).

One objective of this study was to assess whether high precision modeling can discriminate among a limited range of different possible initial S and P concentrations. Although most elements can be modeled effectively for either set of starting parameters, the somewhat better consistency of plots for some element pairs using IP2 (Pt–Os and Re–Ru) suggests that the IVB irons may have crystallized from an initial melt with S closer to 2 wt.% than to 0. This suite of elements, however, does not provide strong constraints on the S content of the initial melt.

4.3. Initial composition and formation of the IVB system

The calculated initial concentrations of the HSE for IP1 and IP2, using parameterized and slope-based D values are provided in Table 5. Composite plots normalized to CI chondrites using initial concentrations estimated from slope-based D values for Re, Os, Pt, Ru and Rh, and initial concentrations estimated for Ir, Pd and Au using the parameterization method are shown in Fig. 14, along with the estimated initial concentration from Campbell and Humayun (2005). Because we strove to minimize the Re concentration as our starting composition parameter, and chose to model Cape of Good Hope and Iquique as forming via the first 5–20% of fractional crystallization, our initial concentrations for some elements, such as Re and Os, are as much as 40% lower than those estimated by Campbell and Humayun (2005) (Table 5). The relative abundances of the HSE, however, are very similar to those estimated by Campbell and Humayun (2005) except that they report a modest enrichment in the chondrite normalized abundance of Pd relative to Rh. Our estimate for the composition of the initial liquid core does not greatly differ from the chemically least evolved IVB iron compositions because of the presumed, relatively low D values for each element that are consistent with a low S + P system. Aside from the depletion in Re relative to Os, the decrease in concentrations of the remaining HSE correlate well with decreases in 50% condensation temperatures. Palladium and Au are considerably less refractory than the other HSE examined here, so their greater depletion relative to the other HSE is also consistent with fractionation occurring as a result of volatility effects.

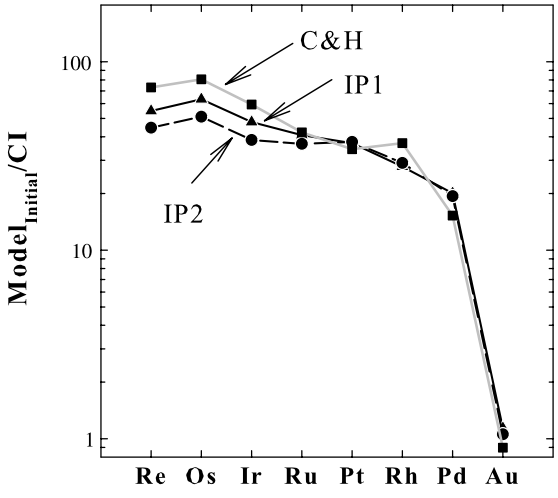

Fig. 14. Plot of calculated initial concentrations of HSE, normalized to CI chondrites in the segregated metal that formed the IVB core. Initial concentrations were calculated for each model as discussed in the text (Table 5). For comparison, the initial concentrations estimated by Campbell and Humayun (2005) are also shown.

Our laser ablation data are generally consistent with those of Campbell and Humayun (2005). The most notable feature in the chondrite normalized plot is the degree of depletion of the volatility trend (Fig. 5). We concur with the findings of Campbell and Humayun (2005) regarding the volatility trend in the data. They noted that no single process of condensation or heating could generate the volatility relation between the elements present in the initial IVB melt. They proposed a multi-step sequence of events to form the IVB parent body. The first stage of formation was characterized by high temperature volatilization and condensation in the solar nebula. This step led to fractionation of refractory siderophile elements (Mo, Ru, Rh, W, Re, Os, Ir, Pt) in metal grains. The next step involved the accretion of the IVB parent body from the refractory metal. Included in this accretion stage were Fe-Ni metal components that may have had refractory siderophile elements that were variably fractionated from one another. The third step in formation was heating of the IVB parent body to a high internal temperature, which resulted in homogenization of the metal components in the parent body.

The relative depletions of the redox sensitive elements W, Mo, V, Fe, Cr, Mn and Cu in most IVB irons is striking (Fig. 5) and provide insights to the degree of oxidization that accompanied core separation in the IVB parent body. Campbell and Humayun (2005) concluded that during metal-silicate separation the oxidization state was approximately IW-1 (1 log unit below the iron wüstite buffer). The depletions of W and Mo in the IVB core, assuming that the core has ~1/3 the mass fraction of the parent body, indicates that ~two-thirds of the budget of W and Mo resided in the silicate portion of the IVB body. Likewise, the marked depletions in V, Cr and Mn in IVB irons are consistent with metal-silicate segregation in the IVB body occurring under much more oxidizing conditions than that for the Earth and, thus, likely produced a IVB silicate shell having significantly elevated abundances of these elements.

The chemical signatures predicted for the silicate shell of the IVB body provide a way by which to consider possible genetic links to known achondrites. A first test of this kind was offered by Campbell and Humayun (2005) who suggested a link with angrite mete orites because both angrites and IVB irons share depletions of moderately volatile elements. Given the reference frame of Earth's core and mantle compositions, we suggest that the bulk silicate portion of the IVB parent body most likely was characterized by Fe/Mn, V/Sc and Mn/Li ratios considerably different from Earth's mantle (~200, 10, 1600, respectively, for the parent body and ~60, 5, 650, respectively for Earth (McDonough, 2003)). Papike et al. (2003) showed that the silicate shell of the angrite parent body had a high Fe/Mn ratio of ~120 which is much higher than that of Earth. However, this elevated Fe/Mn ratio may not be sufficiently high for the bulk silicate portion of the IVB parent body.

Some aspects of the IVB system are still difficult to interpret. In particular, the requirement that the Re/Os and Pt/Os ratios in the initial liquid be substantially lower than the range of chondritic meteorites is particularly vexing. Both Re and Os are susceptible to oxidation, and Os can even form a very volatile tetroxide under highly oxidizing conditions (unlikely in a planetary mantle with metal present). However, there is no evidence of Os removal from the system, and the similarly sub-chondritic Re/Os and Pt/Os ratios of the projected initial liquid are more consistent with Os *enrichment* than Re and Pt depletions. At present we can offer no realistic mechanism for enriching Os in preference to other HSE in metal that is segregating from a relatively oxidized silicate. It must also be considered that the fractionation was a result of nebular processes; however, there is not a viable model for causing such fractionation via condensation or heating for two elements with very similar, extremely refractory characteristics. Nonetheless, there are components in chondrites and even a few bulk chondrites (e.g., Karoonda; Walker et al., 2002) that indicate such fractionations may have occurred as part of a condensation sequence. In light of this apparent condensation temperature control on the markedly subchondritic Re/Os and Pt/Os ratios required for the IVB parent body, a re-examination of the condensation calculations and nebular setting may be useful.

5. CONCLUSIONS

The ^{187}Re–^{187}Os isotopic systematics of all twelve IVB iron meteorites are consistent with closed system behavior of the HSE since the time of crystallization during the earliest portion of solar system history. Our new high-quality HSE data for bulk samples allow for precise modeling of these elements as a function of crystal–liquid fractionation. A simple fractional crystallization model that incorporates changing S and P concentrations and accompanying changes in D values for the HSE and P, can account for all IVB iron bulk compositions as equilibrium solids, liquids, or mixtures of both. The model results suggest the IVB irons crystallized from an initial melt with S closer to 2 wt.% than zero, but the suite of elements examined does not tightly constrain this parameter.

Modeling reveals problems in the application of D values obtained by the parameterization method for compatible HSE, including Re, Os, and Pt, which have generally similar D values. Conversely, slope-based D values fail for the incompatible elements Pd and Au. The successful model can be used to place crude constraints on the proportions of equilibrium solids and liquids present in each meteorite.

In situ analysis of the IVB irons provides corroborating evidence for relatively oxidizing conditions in the parent, consistent with results of previous studies. The ultimate origin of the HSE present in the IVB irons requires complex processing prior to metal segregation but relatively simple crystal–liquid fractionation during crystallization.

ACKNOWLEDGMENTS

Meteorite samples were provided by the Smithsonian Institution National Museum of Natural History, Washington D.C., the Center for Meteorite Studies at Arizona State University, Tempe, the Museum for Naturkunde, Berlin, the American Museum of Natural History, New York, and the Harvard Peabody Museum, Cambridge. These sources of the meteorite specimens are gratefully acknowledged. We thank Mario Luong for his help with data processing in the ICP-MS laboratory. Constructive reviews from D. Cook, H. Haack, M. Humayun and J. Jones are gratefully acknowledged. This material is based upon work supported by NASA under Grant Nos. NNG04GK52G (to R.J.W.), NNG04GG17G (to W.F.M.) and NNG06GI13G (to N.L.C.), issued through the Science Mission Directorate, and by NSF support under Gsrant EAR 0337621 (to W.F.M.).

APPENDIX A. SUPPLEMENTARY DATA

Details of the Chabot and Jones (2003) parameterization used for calculating D values, and additional information regarding analytical procedures and additional comparisons with published data are provided in the Electronic annex. Supplementary data associated with this article can be found, in the online version, at doi:10.1016/j.gca.2008.01.021.

REFERENCES

Achterbergh E. V., Ryan C. G., Jackson S. E. and Griffin W. L. (2001) Appendix 3: Data reduction software for LA-ICP-MS. In: *Laser Ablation-ICP-MS in the Earth Sciences* (ed. P. Sylvester), vol. 29. Mineralogical Association of Canada, Short Course Series, 243 pp.

Anders E. and Grevesse N. (1989) Abundances of the elements: meteoritic and solar. *Geochim. Cosmochim. Acta* **53**, 197–214.

Becker H., Horan M. F., Walker R. J., Gao S., Lorand J.-P. and Rudnick R. L. (2006) Highly siderophile element composition of the Earth's primitive upper mantle: constraints from new data on peridotite massifs and xenoliths. *Geochim. Cosmochim. Acta* **70**, 4528–4550.

Birck J.-L., Roy-Barman M. and Capmas F. (1997) Re–Os isotopic measurements at the femtomole level in natural samples. *Geostand. Newslett.* **20**, 9–27.

Brandon A. D., Walker R. J. and Puchtel I. S. (2006) Platinum–Os isotope evolution of the Earth's mantle: constraints from chondrites and Os-rich alloys. *Geochim. Cosmochim. Acta* **70**, 2093–2103.

Buchwald V. F. (1975) *Handbook of Iron Meteorites*. University of California Press.

Campbell A. J. and Humayun M. (2005) Compositions of group IVB iron meteorites and their parent melt. *Geochim. Cosmochim. Acta* **69**, 4733–4744.

Chabot N. L. and Jones J. H. (2003) Parameterizing iron meteorite partitioning experiments. *Meteorit. Planet. Sci.* **37**, 1425–1436.

Chabot N. L. (2004) Sulfur contents of the parental metallic cores of magmatic iron meteorites. *Geochim. Cosmochim. Acta* **68**, 3607–3618.

Chen J. H. and Wasserburg G. J. (1996). Live ^{107}Pd in the early soalr system and implications for planetary evolution. In *Earth Processes: Reading the Isotopic Code* (eds A. Basu and S. R. Hart), pp. 1–20. Geophysical Monograph 95. American Geophysical Union.

Cohen A. S. and Waters F. J. (1996) Separation of osmium from geological materials by solvent extraction for analysis by thermal ionisation mass spectrometry. *Anal. Chim. Acta* **332**, 269–275.

Cook D. L., Walker R. J., Horan M. F., Wasson J. T. and Morgan J. W. (2004) Pt–Re–Os systematics of group IIAB and IIIAB iron meteorites. *Geochim. Cosmochim. Acta* **68**, 1413–1431.

Creaser R. A., Papanastassiou D. A. and Wasserburg G. J. (1991) Negative thermal ion mass spectrometry of osmium, rhenium, and iridium. *Geochim. Cosmochim. Acta* **55**, 397–401.

Fleet M. E. and Stone W. E. (1991) Partitioning of platinum-group elements in the Fe–Ni–S system and their fractionation in nature. *Geochim. Cosmochim. Acta* **55**, 245–253.

Fleet M. E., Liu M. and Crocket J. H. (1999) Partitioning of trace amounts of highly siderophile elements in the Fe–Ni–S system and their fractionation in nature. *Geochim. Cosmochim. Acta* **63**, 2611–2622.

Hamester M., Wiederin D., Wills J., Kerl W. and Douthitt C. B. (1999) Strategies for isotope ratio measurements with a double focusing sector þ eld ICP-MS. *Fresen. J. Anal. Chem.* **364**, 495497.

Horan M. F., Smoliar M. I. and Walker R. J. (1998) ^{182}W and ^{187}Re–^{187}Os systematics of iron meteorites: chronology for melting, differentiation and crystallization in asteroids. *Geochim. Cosmochim. Acta* **62**, 545–554.

Horan M. F., Walker R. J., Morgan J. W., Grossman J. N. and Rubin A. (2003) Highly siderophile elements in chondrites. *Chem. Geol.* **196**, 5–20.

Jones J. H. and Drake M. J. (1983) Experimental investigation of trace element fractionation in iron meteorites. II: The influence of sulfur. *Geochim. Cosmochim. Acta* **47**, 1199–1209.

Jones J. H. and Malvin D. J. (1990) A nonmetal interaction model for the segregation of the trace metals during solidification of Fe–Ni–S, Fe–Ni–P, Fe–Ni–S–P alloys. *Metall. Trans. B* **21B**, 697–706.

Kelly W. R. and Larimer J. W. (1977) Chemical fractionations in meteorites-VIII. Iron meteorites and the cosmochemical history of the metal phase. *Geochim. Cosmochim. Acta* **41**, 93–111.

Luck J.-M., Birck J.-L. and Allegre C.-J. (1980) ^{187}Re–^{187}Os systematics in meteorites: early chronology of the Solar System and age of the galaxy. *Nature* **283**, 256–259.

Luck J.-M. and Allègre C.-J. (1983) ^{187}Re–^{187}Os systematics in meteorites and cosmochemical consequences. *Nature* **302**, 130–133.

Ludwig K. R. (2003) User's Manual for Isoplot 3.00. Berkeley Geochronology Center Special Publication No. 4, Berkeley, CA, 70 pp.

McDonough W. F. (2003) Compositional model for the Earth's core. In *The Mantle and Core*, vol. 2 (eds. R. W. Carlson, H. D. Holland and K. K. Turekian), pp. 547–568. Treatise on Geochemistry. Elsevier-Pergamon, Oxford.

Morgan J. W., Horan M. F., Walker R. J. and Grossman J. N. (1995) Rhenium–osmium concentration and isotope systematics in group IIAB iron meteorites. *Geochim. Cosmochim. Acta* **59**, 2331–2344.

Papike J. J., Karner J. M. and Shearer C. K. (2003) Determination of planetary basalt parentage: a simple technique using the electron microprobe. *Am. Mineral.* **88**, 469–472.

Pernicka E. and Wasson J. T. (1987) Ru, Re, Os, Pt, and Au in iron meteorites. *Geochim. Cosmochim. Acta* **51**, 1717–1726.

Petaev M. I. and Jacobsen S. B. (2004) Differentiation of metal-rich meteoritic parent bodies: I. Measurements of PGE's, Re, Mo, W, and Au in meteoritic Fe–Ni metal. *Meteorit. Planet. Sci.* **39**, 1685–1697.

Rasmussen K. L., Malvin D. J., Buchwald V. F. and Wasson J. T. (1984) Compositional trends and cooling rates of group-IVB iron meteorites. *Geochim. Cosmochim. Acta* **48**, 805–813.

Rehkämper M. and Halliday A. N. (1997) Development and application of new ion-exchange techniques for the separation of the platinum group and other siderophile elements from geological samples. *Talanta* **44**, 663–672.

Schaudy R., Wasson J. T. and Buchwald V. F. (1972) Chemical classification of iron meteorites: 6. A reinvestigation of irons with Ge concentrations lower than 1 ppm. *Icarus* **17**, 174–192.

Scherstén A., Elliott T., Hawkesworth C., Russell S. and Masarik J. (2006) Hf-W evidence for rapid differentiation of iron meteorite parent bodies. *Earth Planet. Sci. Lett.* **241**, 530–542.

Scott E. R. D. (1972) Chemical fractionation in iron meteorites and its interpretation. *Geochim. Cosmochim. Acta* **36**, 1205–1236.

Shen J. J., Papanastassiou D. A. and Wasserburg G. J. (1996) Precise Re–Os determinations and systematics in iron meteorites. *Geochim. Cosmochim. Acta* **60**, 2887–2900.

Shirey S. B. and Walker R. J. (1995) Carius tube digestion for low-blank rhenium–osmium analysis. *Anal. Chem.* **67**, 2136–2141.

Smoliar M. I., Walker R. J. and Morgan J. W. (1996) Re–Os ages of group IIA, IIIA, IVA, and IVB iron meteorites. *Science* **271**, 1099–1102.

Walker R. J., Morgan J. W., Beary E., Smoliar M. I., Czamanske G. K. and Horan M. F. (1997) Applications of the ^{190}Pt–^{186}Os isotope system to geochemistry and cosmochemistry. *Geochim. Cosmochim. Acta* **61**, 4799–4808.

Walker R. J., Horan M. F., Morgan J. W., Becker H., Grossman J. N. and Rubin A. (2002) Comparative ^{187}Re–^{187}Os systematics of chondrites: implications regarding early solar system processes. *Geochim. Cosmochim. Acta* **66**, 4187–4201.

Wasson J. T. (1974) *Meteorites: Classification and Properties*. Springer-Verlag.

Wasson J. T. (1999) Trapped melt in IIIAB irons; solid/liquid elemetal partitioning during the fractionation of the IIIAB magma. *Geochim. Cosmochim. Acta* **63**, 2875–2889.

Wasson J. T. and Richardson J. W. (2001) Fractionation trends among IVA iron meteorites: contrasts with IIIAB trends. *Geochim. Cosmochim. Acta* **65**, 951–970.

Wasson J. T., Huber H. and Malvin D. J. (2007) Formation of IIAB iron meteorites. *Geochim. Cosmochim. Acta* **71**, 760–781.

Yin Q. Z., Jacobsen S. B., Lee C.-T., McDonough W. F., Rudnick R. L. and Horn I. (2001) A gravimetric K_2OsCl_6 standard: application to precise and accurate Os spike calibration. *Geochim. Cosmochim. Acta* **65**, 2113–2127.

Associate editor: Gregory F. Herzog